Published for SISSA by Springer

Received: *May 3, 2018*
Accepted: *November 11, 2018*
Published: *November 23, 2018*

NNLOPS accurate associated HZ production with H→ $b\bar{b}$ decay at NLO

William Astill,[a] **Wojciech Bizoń,**[a] **Emanuele Re**[b,c] **and Giulia Zanderighi**[a,c]

[a] *Rudolf Peierls Centre for Theoretical Physics, Clarendon Laboratory, Parks Road, Oxford, U.K.*

[b] *LAPTh, CNRS, Université Savoie Mont Blanc, 74940 Annecy, France*

[c] *Theoretical Physics Department, CERN, Geneva, Switzerland*

E-mail: william.astill@physics.ox.ac.uk, wojciech.bizon@physics.ox.ac.uk, emanuele.re@lapth.cnrs.fr, giulia.zanderighi@cern.ch

Abstract: We present a next-to-next-to-leading order (NNLO) accurate description of associated HZ production, followed by the Higgs boson decay into a pair of b-quarks treated at next-to-leading order (NLO), consistently matched to a parton shower (PS). The matching is achieved by performing reweighting of the `HZJ-MiNLO` events, using multi-dimensional distributions that are fully-differential in the HZ Born kinematics, to the NNLO results obtained by using the `MCFM-8.0` fixed-order calculation. Additionally we include the $gg \to$HZ contribution to the discussed process that appears at the $\mathcal{O}(\alpha_s^2)$. We present phenomenological results obtained for 13 TeV hadronic collisions.

Keywords: NLO Computations, QCD Phenomenology

ArXiv ePrint: 1804.08141

https://doi.org/10.1007/JHEP11(2018)157

JHEP11(2018)157

Contents

1 Introduction

After the discovery of the Higgs boson in Run I [1, 2], one of the main tasks of the ongoing LHC Run II is to perform accurate measurements of Higgs properties. In order to carry out this precision physics program, it is important to study Higgs production in all the main production modes, and compare measurements with theory predictions, for total cross sections and differential distributions. An important goal which is expected to be achievable with the Run II full luminosity is to establish solid statistical evidence for HV associated production [3, 4].

The past years have seen a remarkable progress in NNLO QCD calculations, and, currently, all $2 \to 2$ SM scattering processes are known to this accuracy, see e.g. ref. [5]. Thanks to this progress, the description of colour singlet final states has reached a high level of accuracy. This is particularly true for processes where, at leading order (LO), there are no gluons in the initial state: in this case higher-order corrections are typically moderate, and hence including NNLO corrections leads to very stable results, with small perturbative uncertainties. For HZ production, the NNLO corrections have been computed for the inclusive cross section [6] as well as for differential distributions [7–9]. Electroweak corrections for this process are also known at NLO for inclusive cross sections and differential distributions [10, 11], and are implemented in the public code `HAWK` [12]. Notably, NLO electroweak and QCD corrections were simultaneously matched to a parton shower in ref. [13] for HV and HV+jet, using, in the latter case, the `MiNLO` method (to be described below).

Since associated HV production has a small cross section, it is often considered in association with a Higgs boson decaying to a b-quark pair, which is the largest Higgs decay mode. In this case properties of the b-jets arising from the Higgs decay products are used in experimental analysis to enhance the signal over SM backgrounds, and they will also be important for extracting precise information on the b-quark Yukawa coupling, especially in the Higgs boosted regime. Because of this, including QCD corrections to the $\mathrm{H} \to b\bar{b}$ decay is particularly important, especially since these corrections are known to be large. The QCD NLO corrections to the Higgs decay to massive b-quarks have been known for a long time [14–18], whereas more recently NNLO corrections were computed in refs. [19, 20] for massless b-quarks. In the last few years the focus has moved towards a combination of the aforementioned fully-differential NNLO computations for $pp \to \mathrm{HV}$ with differential NLO and NNLO results for $\mathrm{H} \to b\bar{b}$. The current state-of-the-art results are those obtained in refs. [9, 21], where the fully-differential QCD NNLO computations for $pp \to \mathrm{HV}$ and $\mathrm{H} \to b\bar{b}$ (in the limit of massless b-quarks) have been combined together.

The precision of theory predictions is usually quantified in terms of renormalisation and factorisation scale variation of the NNLO results. It is however also known that all-order effects can be sizeable and can give rise to effects that are outside the fixed-order scale uncertainty band. For this reason, a lot of effort is put into combining NNLO calculations with parton shower effects, thereby obtaining so-called NNLOPS generators. Three methods have been suggested recently to achieve this accuracy. The `UNNLOPS` approach, which has been used for Drell-Yan [22] and Higgs production [23], is based on partitioning the phase space into an unresolved and a one-jet region and a subsequent matching to parton shower for the resolved one-jet region. The `Geneva` approach [24] instead uses the next-to-next-to-leading logarithmic (NNLL) accurate resummation for a specific observable to essentially partition the phase space. This method has been applied recently to Drell-Yan production [24]. Finally, the `MiNLO` approach [25, 26] relies on first using `MiNLO` to achieve an NLO merging of the processes with the production of the colour-singlet state (X) and the same processes with one additional jet ($X + 1$ jet), and on performing a reweighing of the `MiNLO` $X + 1$ jet events to NNLO Born distributions for X. This method has been applied recently to Higgs production [27, 28], Drell-Yan [29] and HW production [30].

In this paper we consider the production of a Higgs boson in association with a Z boson and consider the decay of the Higgs to bottom quarks, the decay mode with the largest branching ratio, and the decay of the Z boson to leptons. We build a Monte Carlo that is NNLO accurate in production, preserves NLO accuracy in the decay and includes parton shower effects.[1] In order to do so, we start by implementing, in the `POWHEG-BOX-RES` framework, a `MiNLO`-improved simulation of `HZJ`, similar to the one already available in `POWHEG-BOX-V2`, and presented in ref. [32]. We also include the NNLO $gg \to$HZ channel at leading order in production, including LO corrections in decay and parton shower effects. This subprocesses is added separately, and we assess its numerical impact. Our implementation uses and adapts the `POWHEG-BOX-RES` code, which is based on `POWHEG-BOX-V2` but has a resonant-aware treatment of internal resonances [33], and hence it is suited to treat NLO corrections to production and decay.

The paper is organised as follows. In section 2 we outline the method used to obtain `NNLOPS` accurate predictions including the NLO treatment of the decay. In particular we explain how the latter is included together with `MiNLO` within the `POWHEG-BOX-RES` framework. We detail how we parametrise the phase-space, and also explain how we treat the $\mathcal{O}(\alpha_s^2)$ $gg \to$HZ contribution. In section 3 we give details about our practical implementation, as well as about our interface to the parton shower. In section 4 we validate our results by checking that we reproduce NNLO results for Born-like observables, also for variables not used for the reweighting. In section 5 we present distributions with fiducial cuts inspired by the recent ATLAS analysis of ref. [3]. Finally, we present our conclusions in section 6. A number of appendices provide more details about the treatment of the decay at NLO, the spectral decomposition that we use to parametrise the phase space, the dependence of the matrix element on the extra polar angle used in the phase-space parametrisation, and the impact of $gg \to$HZ contribution.

2 Outline of the method

In this work we consider the production of a Higgs boson in association with a Z boson, followed by the Z boson decay into a pair of leptons and the Higgs boson decay into pair of b-quarks

$$pp \longrightarrow HZ \longrightarrow \left(b\bar{b}\right)\left(\ell^+\ell^-\right). \tag{2.1}$$

The decay of the Z boson is treated exactly with all spin correlations between initial and final-state fermions taken into account. The decay of the Higgs boson is treated exactly too: the Higgs boson propagator has been fully kept, and we use the fact that the matrix elements for production and decay exactly factorise in this case.

In order to achieve `NNLOPS` accuracy we follow the method of reweighting Les Houches events (`LHE`), produced by `MiNLO` improved `HZJ` generator (`HZJ-MiNLO`), with NNLO accurate fixed-order predictions, differential in the Born phase space. The procedure was first proposed in [26] and later implemented for various colour-singlet production processes [27–30]. In its simplest implementation, the method consists in reweighting `LHE` event samples obtained with the `HZJ-MiNLO` generator using multi-differential `HZNNLO` distributions, with the factor

$$\mathcal{W}(\Phi_{\ell\bar{\ell}b\bar{b}}) = \frac{d\sigma_{\texttt{NNLO}}(\Phi_{\ell\bar{\ell}b\bar{b}})}{d\sigma_{\texttt{MiNLO}}(\Phi_{\ell\bar{\ell}b\bar{b}})}, \tag{2.2}$$

[1] We note that **Herwig++** code also allows to include NLO corrections to the $H \to bb$ decay in HV production [31].

JHEP11(2018)157

where $\Phi_{\ell\bar{\ell}b\bar{b}}$ is the Born phase-space of process (2.1). The resulting event sample (which we refer to by `HZ-NNLOPS(LHEF)`) is NNLO accurate: by construction the method provides NNLO accuracy for all Born distributions and 1-jet observables remain NLO accurate since the reweighting factor differs from one by $\mathcal{O}(\alpha_s^2)$ corrections. For the proof we refer the reader to [27, 29]. Furthermore, a subsequent parton shower will not spoil the claimed accuracy provided that the hardest real radiation for each event is generated by `POWHEG` itself. This procedure was applied recently to HW production in ref. [30], hence we refer the reader to that paper for further details. Instead, in this section, we first give a detailed description of the treatment of the NLO $\mathrm{H} \to b\bar{b}$ decay, which is the new element of this work (section 2.1). We then give some technical details on how the reweighting to NNLO was achieved (section 2.2 and 2.3), and, finally, in section 2.4 we discuss the inclusion of the loop-induced $gg \to \mathrm{HZ}$ process, which is part of the NNLO corrections to $pp \to \mathrm{HZ}$.

2.1 `HZJ-MiNLO` with $\mathrm{H} \to b\bar{b}$ decay at NLO

In this work we use the `MiNLO` prescription only for the production part of the process, and match this to a "resonance improved" `POWHEG` implementation of the NLO QCD calculation of the $\mathrm{H} \to b\bar{b}$ decay. The motivation for using a "resonance improved" `POWHEG` matching scheme will be discussed in section 3.1, while here we will focus on details of the `MiNLO` formula in the presence of a resonance.

We start by introducing the $\bar{B}$ function [34] that we use in our `HZJ` code, which reads schematically

$$\begin{aligned}\bar{B} = \alpha_s(q_t^2)\Delta_q^2(Q,q_t)\frac{\mathrm{Br}(\mathrm{H}\to b\bar{b})}{\Gamma_{\mathrm{NLO}}}\Bigg[&B_{\mathrm{HZJ}}(1-2\Delta_q^{(1)}(Q,q_t))d\Gamma_{b\bar{b}}^{(0)} \\ &+\left(V_{\mathrm{HZJ}}+\int d\phi_r R_{\mathrm{HZJ}}(\phi_r)\right)d\Gamma_{b\bar{b}}^{(0)}+B_{\mathrm{HZJ}}\left(d\Gamma_{b\bar{b}}^{(V)}+\int d\phi_r d\Gamma_{b\bar{b}}^{(R)}(\phi_r)\right)\Bigg],\end{aligned} \tag{2.3}$$

where the Higgs propagator is left implicit; $\mathrm{Br}(\mathrm{H} \to b\bar{b})$ is the best prediction for the Standard Model $\mathrm{H} \to b\bar{b}$ branching ratio; and $d\Gamma_{b\bar{b}}^{(0/V/R)}$ are the Born, virtual, and real squared amplitudes for the $\mathrm{H} \to b\bar{b}$ decay, differential in their kinematics. $\Gamma_{\mathrm{NLO}} = \Gamma_{b\bar{b}}^{(0)} + \Gamma_{b\bar{b}}^{(1)}$ denotes the NLO accurate $\mathrm{H} \to b\bar{b}$ partial decay width. With $\Delta_q(Q, q_t)$ we denote the `MiNLO` Sudakov form factor for quark induced boson production (see ref. [26] for its precise definition) and $\Delta_q^{(1)}(Q, q_t)$ is its $\mathcal{O}(\alpha_s)$ expansion. The hard scale in the `MiNLO`-Sudakov is set to $Q^2 = (p_Z + p_H)^2$ and q_t is the transverse momentum of the HZ system, where the Higgs momentum is obtained from the sum of the momenta of its decay products ($b\bar{b}$ or $b\bar{b}g$). In the formula above the additional α_s factor in the NLO correction is contained implicitly in the V and R functions, as well as in $d\Gamma_{b\bar{b}}^{(V)}$ and $d\Gamma_{b\bar{b}}^{(R)}$. In the former two, following the `MiNLO` prescription, we set the central renormalisation scale to $\mu_R = q_t$, whereas for the decay we set the central scale to $\mu_{\mathrm{R}} = M_{\mathrm{H}}$ since this is the natural scale for the decay and no `MiNLO` procedure is applied to it (in appendix A we denote as μ_r the renormalisation scale for the decay).

If we integrate eq. (2.3) over the phase space of all final-state light partons we obtain

$$d\sigma_{\mathtt{MiNLO}}(\Phi_{\ell\bar{\ell}b\bar{b}}) = \mathrm{Br}(\mathrm{H}\to b\bar{b})\cdot\left[\left(d\sigma^{(0)}_{\mathrm{HZ}} + d\sigma^{(1)}_{\mathrm{HZ}}\right)\cdot\frac{d\Gamma^{(0)}_{b\bar{b}} + d\Gamma^{(1)}_{b\bar{b}}}{\Gamma_{\mathrm{NLO}}} + d\tilde{\sigma}^{(2)}_{\mathrm{HZ}}\cdot\frac{d\Gamma^{(0)}_{b\bar{b}}}{\Gamma_{\mathrm{NLO}}}\right] + \mathcal{O}(\alpha_s^3), \tag{2.4}$$

where

$$d\Gamma^{(1)}_{b\bar{b}} = d\Gamma^{(V)}_{b\bar{b}} + \int d\phi_r d\Gamma^{(R)}_{b\bar{b}}(\phi_r)\,, \tag{2.5}$$

and $d\sigma^{(i)}_{\mathrm{HZ}}$ denotes the $\mathcal{O}(\alpha_s^i)$ correction to the HZ production cross section. The $d\tilde{\sigma}^{(2)}$ denotes the $\mathcal{O}(\alpha_s^2)$ part of the `HZJ-MiNLO` computation, which corresponds to double-real and real-virtual parts of HZ production at NNLO.

We obtain NNLO prediction (*without* the loop-induced $gg\to\mathrm{HZ}$ contribution, which is discussed in section 2.4) for the production combined with NLO corrections to the decay from `MCFM-8.0`, whose output is

$$d\sigma_{\mathtt{NNLO}}(\Phi_{\ell\bar{\ell}b\bar{b}}) = \mathrm{Br}(\mathrm{H}\to b\bar{b})\cdot\left[d\sigma^{(0)}_{\mathrm{HZ}}\cdot\frac{d\Gamma^{(0)}_{b\bar{b}} + d\Gamma^{(1)}_{b\bar{b}}}{\Gamma_{\mathrm{NLO}}} + (d\sigma^{(1)}_{\mathrm{HZ}} + d\sigma^{(2)}_{\mathrm{HZ}})\cdot\frac{d\Gamma^{(0)}_{b\bar{b}}}{\Gamma^{(0)}_{b\bar{b}}}\right]. \tag{2.6}$$

It is easy to check that after integrating out the decay of the Higgs boson in equation (2.6) one recovers the fully inclusive NNLO result multiplied by the overall branching ratio. One can also easily verify that

$$\mathcal{W}(\Phi_{\ell\bar{\ell}b\bar{b}}) = \frac{d\sigma_{\mathtt{NNLO}}(\Phi_{\ell\bar{\ell}b\bar{b}})}{d\sigma_{\mathtt{MiNLO}}(\Phi_{\ell\bar{\ell}b\bar{b}})} = 1 + \frac{\left(\sigma^{(2)} - \tilde{\sigma}^{(2)}\right)}{\sigma^{(0)}} + \mathcal{O}\left(\alpha_{\mathrm{s}}^3\right)\,, \tag{2.7}$$

which means that reweighting `HZJ-MiNLO` events with this factor does not spoil the NLO accuracy of the event sample in the HZ+jet region, since the rescaling is equal to one up to $\mathcal{O}(\alpha_{\mathrm{s}}^2)$ terms. In the following section we describe how we proceed to obtain distributions differential in the Born phase space $\Phi_{\ell\bar{\ell}b\bar{b}}$.

2.2 Phase-space parametrisation

Our Born phase space contains four final-state particles, two leptons (ℓ^+, ℓ^-) and two bottom quarks $(b, \bar{b})$. After neglecting an irrelevant azimuthal angle and upon inclusion of the initial-state degrees of freedom we are left with 9 independent dimensions. Furthermore we can factorise the Born phase-space as follows:

$$d\Phi_{\ell\bar{\ell}b\bar{b}} = d\Phi_{\mathrm{H}\ell\bar{\ell}} \times (2\pi)^3 dq^2 \times d\Phi_{H\to b\bar{b}}, \tag{2.8}$$

where q^2 is the virtuality of the Higgs boson, $\Phi_{\mathrm{H}\ell\bar{\ell}}$ is the 6-dimensional phase space for the production of an undecayed Higgs boson with a pair of leptons from the decay of the associated Z boson, and $\Phi_{H\to b\bar{b}}$ is the 2-dimensional phase space for the decay of a Higgs boson into a pair of b-quarks. We perform a reweighting only on the first part of the phase-space $\Phi_{\mathrm{H}\ell\bar{\ell}}$, as the Higgs is a very narrow resonance, and its decay is already treated at the required accuracy (NLO) in our implementation of `HZJ-MiNLO`.

A parametrisation of $\Phi_{\mathrm{H}\ell\bar{\ell}}$ can be defined in a number of ways. After careful considerations we have chosen the invariant mass and rapidity of the HZ system (M_{HZ} and y_{HZ}) to be the first two variables. As a third variable we choose $\cos\alpha$, where α is the polar angle of the Z boson with respect to the beam axis in the frame where the HZ system is at rest, i.e.

$$\cos\alpha = \frac{\vec{p}\,'_Z \cdot \hat{z}'}{|\vec{p}\,'_Z|\,|\hat{z}'|}, \tag{2.9}$$

where $'$ indicates that directions are expressed in the HZ rest-frame and the original $\hat{z}$ direction is along the beam axis. Subsequently we choose the invariant mass of the Z boson, $M_{\ell\bar{\ell}}$, and a convenient choice for the last two dimensions is to use Collins-Soper angles (θ^*, ϕ^*) defined in [35]. In summary the full phase space parametrisation reads

$$\Phi_{\mathrm{H}\ell\bar{\ell}} = \{M_{\mathrm{HZ}}, y_{\mathrm{HZ}}, \cos\alpha, M_{\ell\bar{\ell}}, \theta^*, \phi^*\}\,. \tag{2.10}$$

Following the arguments of [35] and the discussion in section 2 of [30] we parametrise the (θ^*, ϕ^*)-dependence as follows:

$$\begin{aligned}\frac{d\sigma}{d\Phi_{\mathrm{H}\ell\bar{\ell}}} &= \frac{d^6\sigma}{dM_{\mathrm{HZ}}\,dy_{\mathrm{HZ}}\,d\cos\alpha\,d\cos\theta^* d\phi^*}\\ &= \frac{3}{16\pi}\left(\frac{d\sigma}{d\Phi_{\mathrm{HZ}}}(1+\cos^2\theta^*) + \sum_{i=0}^{7} A_i(\Phi_{\mathrm{HZ}}) f_i(\theta^*, \phi^*)\right)\,,\end{aligned} \tag{2.11}$$

where in the second line we have used a short notation for the phase-space without leptonic angles

$$\Phi_{\mathrm{HZ}} = \{M_{\mathrm{HZ}}, y_{\mathrm{HZ}}, \cos\alpha\}\,. \tag{2.12}$$

The complete set of functions $f_i(\theta^*, \phi^*)$, together with a procedure for extracting coefficients $A_i(\Phi_{\mathrm{HZ}})$, is given in equations (2.3-2.4) of ref. [30]. We note that for practical purposes we will use only the first five A_i coefficients ($A_0, \ldots A_4$) and, for simplicity, we neglect the remaining three (A_5, A_6, A_7) since their impact on any distribution that we examined is numerically negligible.

Finally, we can parametrise the dependence on the Z boson polar angle α (see eq. (2.9)) using a set of orthonormal functions $g_j(\cos\alpha)$. The definition of the basis elements g_j is given in appendix B. With this choice we have

$$\begin{aligned}\frac{d\sigma}{d\Phi_{\mathrm{HZ}}} &= \sum_{j=0}^{N} c_j(\Phi)\, g_j\,(\cos\alpha)\,,\\ A_i\,(\Phi_{\mathrm{HZ}}) &= \sum_{j=0}^{N} a_{ij}(\Phi)\, g_j\,(\cos\alpha)\,,\end{aligned} \tag{2.13}$$

where c_j and a_{ij} are coefficients depending on $\Phi = \{M_{\mathrm{HZ}}, y_{\mathrm{HZ}}\}$ and N is the upper limit of the sum, which in general can be inferred by analysing the matrix elements contributing to the cross section. We investigate the matrix elements in appendix C and find that, at most, polynomials of 5th-degree in the $\cos\alpha$ and $\sin\alpha$ variables can appear. Accordingly, we set $N = 10$ in eq. (2.13).

To summarise, our parametrisation of the fully differential cross section as used in the reweighting procedure reads

$$\frac{d\sigma}{d\Phi_{\mathrm{H}\ell\bar{\ell}}} = \frac{3}{16\pi} \sum_{j=0}^{10} \left(c_j(\Phi)\,(1+\cos^2\theta^*) + \sum_{i=0}^{7} a_{ij}(\Phi)\, f_i(\theta^*,\phi^*) \right) g_j\,(\cos\alpha)\;, \tag{2.14}$$

where the functions $g_j(\cos\alpha)$ are defined in eq. (B.5) and the coefficients $c_j(\Phi)$ and $a_{ij}(\Phi)$ can be obtained from eq. (2.13) by exploiting the orthonormality of the g_j functions.

2.3 Reweighting procedure

The reweighting procedure schematically described so far leaves some degree of freedom. The simple rescaling with a factor, presented in (2.2), spreads the corrections uniformly over the whole phase-space. However we know that regions where the HZ system is accompanied by hard QCD radiation is equally well described by both predictions, `HZNNLO` and `HZJ-MiNLO`. Hence, it is desirable to limit the corrections to the phase space with no hard jet. To achieve this, we proceed along the lines of the prescription presented in [27]. We split the cross section into two parts

$$d\sigma_A = d\sigma\, h(p_t), \qquad d\sigma_B = d\sigma\,(1-h(p_t))\,, \tag{2.15}$$

where

$$h(p_t) = \frac{(M_{\mathrm{H}}+M_{\mathrm{Z}})^2}{(M_{\mathrm{H}}+M_{\mathrm{Z}})^2+p_t^2}\,, \tag{2.16}$$

and p_t is the transverse momentum of the leading jet, computed here using the k_t-algorithm with $R = 0.4$. With such a choice eq. (2.2) takes form

$$\begin{aligned}\mathcal{W}(\Phi_{\mathrm{H}\ell\bar{\ell}}, p_t) \;=\; & h(p_t)\,\frac{\int d\sigma_{\mathtt{NNLO}}\,\delta(\Phi_{\mathrm{H}\ell\bar{\ell}}-\Phi_{\mathrm{H}\ell\bar{\ell}}(\Phi)) - \int d\sigma_{\mathtt{MiNLO},B}\,\delta(\Phi_{\mathrm{H}\ell\bar{\ell}}-\Phi_{\mathrm{H}\ell\bar{\ell}}(\Phi))}{\int d\sigma_{\mathtt{MiNLO},A}\,\delta(\Phi_{\mathrm{H}\ell\bar{\ell}}-\Phi_{\mathrm{H}\ell\bar{\ell}}(\Phi))} \\ & + (1-h(p_t))\,. \end{aligned} \tag{2.17}$$

This procedure smoothly turns off the corrections when moving to regions of phase space with hard emissions whilst preserving the total cross section,

$$\left(\frac{d\sigma}{d\Phi_{\mathrm{H}\ell\bar{\ell}}}\right)_{\mathtt{NNLOPS}} = \left(\frac{d\sigma}{d\Phi_{\mathrm{H}\ell\bar{\ell}}}\right)_{\mathtt{NNLO}}. \tag{2.18}$$

It is worth noting that choosing the transverse momentum p_t in eq. (2.16) as the transverse momentum of hardest jet is not equivalent to choosing the transverse momentum of the colour-singlet, the difference being due to configurations where the colour-singlet has small transverse momentum and it is accompanied by hard QCD emissions whose transverse momenta counterbalance each other. The latter configurations dominate in the region where $p_{t,\mathrm{HZ}} \sim 0$.

In the next section we will explain how we have included in our simulation the loop-mediated $gg \to \mathrm{HZ}$ contribution, which was not included in $d\sigma_{\mathtt{NNLO}}$ (and hence not even in the reweighting factor defined in eq. (2.17)), whilst being formally $\mathcal{O}(\alpha_s^2)$.

2.4 Treatment of the $gg \to \mathrm{HZ}$ contribution

The $\mathcal{O}(\alpha_s^2)$ contributions of the form $gg \to \mathrm{HZ}$, that appear in the process of Higgs boson production in association with a Z boson, originate from the squared 1-loop diagrams shown for example in figure 5 of ref. [8]. There are two classes of contributions: box diagrams involving a Yukawa coupling of the Higgs boson, and triangle diagrams where the Higgs boson is radiated from the Z boson which couples to the fermion loop. Both contributions vanish trivially when massless quarks of the first and second generation run in the loop. These $gg \to \mathrm{HZ}$ contributions are known to constitute a significant part of the cross section [7, 8, 21, 36, 37], especially when the invariant mass of the produced HZ system is larger than twice the top-quark mass. Being loop-induced, so far only approximate NLO corrections are known for this channel [38, 39]. On the other hand, their loop origin makes these terms particularly sensitive to New Physics [40–42].

In our reweighting procedure we do not include this contribution, but we will treat it independently using a separate event sample produced using a leading order implementation of loop-induced $gg \to \mathrm{HZ}$ process implemented in `POWHEG` [32], which includes top and bottom quarks in the loop.[2] We note that the $gg \to \mathrm{HZ}$ contribution can be treated separately since it is finite. Furthermore, parton shower radiation from gluon-initiated hard processes is typically different from processes also involving initial-state quarks. From that point of view, it is important not to include the $gg \to \mathrm{HZ}$ contribution through a simple reweighting. Further discussion of the $gg \to \mathrm{HZ}$ channel is presented in appendix D. For this contribution we do not include any radiative correction to the the $\mathrm{H} \to b\bar{b}$ decay, hence the radiation from the decay is fully taken care of by `Pythia8`. Higher-order NLO corrections to this decay could also be included with relatively little effort.

3 Practical implementation

In this section we first discuss the codes used to obtain our predictions, as well as the relevant settings and the parameters. We also describe subtleties related to the interface to `Pythia8` when radiation from resonances is taken into account.

3.1 Codes and settings

In order to obtain an ensemble of NNLOPS accurate Les Houches events for the process in eq. (2.1) we need fully differential predictions from an NNLO fixed-order calculation, and an NLO accurate event-sample for `HZJ` production improved with the `MiNLO` prescription.

For the NNLO fixed-order prediction we use the `MCFM-8.0` calculation [8]. In order to obtain both the NNLO accuracy for the production of the HZ resonance as well as the NLO accuracy of hadronic decay of Higgs boson, $\mathrm{H} \to b\bar{b}$, we perform two separate runs of the program with `nproc=101` at the `'nnlo'` order (for the first) and `nproc=1010` at the `'nlo'` order (for the latter). The prediction presented in eq. (2.6) is simply obtained by adding the results of the two runs. As it was pointed out in section 2.1 and section 2.4, we do not include $gg \to \mathrm{HZ}$ contributions in the reweighting procedure. To remove them

[2]The code can be obtained from svn://powhegbox.mib.infn.it/trunk/User-Processes-V2/ggHZ.

we have modified part of the MCFM-8.0 code, which computes double-virtual corrections. We will include this contribution in our phenomenological analysis in section 5, as stated clearly in the appropriate places.

The initial sample of Les Houches events is generated using the HZJ-MiNLO package, originally in POWHEG-BOX-V2, which we adapted to run in POWHEG-BOX-RES [33]. We have also extended the original package to include NLO corrections of the Higgs boson decay into a pair of b-quarks, as discussed in section 2.1. The relevant matrix elements have been reported in appendix A. Despite the fact that there is no interference between production and decay, in order to treat the radiation from the resonance we have made use of the POWHEG-BOX-RES framework [33]. As explained in refs. [33, 43], we stress that, even if the Higgs is a narrow and colourless resonance, it is nevertheless necessary to use a resonance-aware procedure when matching (N)NLO and parton showers, in order to guarantee that the mapping from the underlying Born phase space to the radiation phase space preserves the off-shellness of the intermediate resonance. While we could have used the novel resonance-aware routines available in POWHEG-BOX-V2, we have chosen to use the POWHEG-BOX-RES framework which is likely to become the standard going forward. We note that, since in this particular case there is no interference between radiation from the production stage and the Higgs resonance, we have assigned by hand the resonance structure. This has the advantage that the POWHEG-BOX-RES machinery does not need to assign a weight to the resonance history based on its Breit Wigner structure.

In our work we use PDF4LHC15_nnlo_mc parton distribution functions [44–47]. We set $M_{\mathrm{H}} = 125.0\,\mathrm{GeV}$, $\Gamma_H = 4.088\,\mathrm{MeV}$, $M_{\mathrm{Z}} = 91.1876\,\mathrm{GeV}$, and $\Gamma_Z = 2.4952\,\mathrm{GeV}$. Moreover $G_F = 1.16639{\cdot}10^{-5}\,\mathrm{GeV}^{-2}$, $\sin^2\theta_W = 0.2223$, $\alpha_{\mathrm{EM}}(M_{\mathrm{Z}}) = 128.89$, and $\mathrm{Br}(\mathrm{H}\to b\bar{b}) = 0.5824$.

For the contributions where the Higgs boson is radiated from a heavy-quark loop we use the pole mass of the heavy quark, as is usually done in publicly available codes [8]. In particular we set the pole mass of the bottom quark to $m_b = 4.92\,\mathrm{GeV}$ and the pole mass of the top quark to $m_t = 173.2\,\mathrm{GeV}$. Moreover, for the bottom Yukawa coupling in $\mathrm{H}\to b\bar{b}$ decay we use its $\overline{\mathrm{MS}}$ running mass evaluated at scale M_{H}. The running masses are computed from the pole masses using an $\mathcal{O}(\alpha_s^2)$ conversion [48] and the numerical value of the $\overline{\mathrm{MS}}$ mass for the bottom quark, obtained by running the strong coupling using LHAPDF, is $m_b(M_{\mathrm{H}}) = 3.16\,\mathrm{GeV}$.

The NNLO fixed-order prediction is obtained using fixed renormalisation and factorisation scale equal to sum of the Higgs boson and the Z boson mass, $\mu = M_{\mathrm{H}} + M_{\mathrm{Z}}$. In HZJ-MiNLO the scale choice for the production is fixed by the MiNLO procedure [25], while for the decay the central scale choice is M_{H}, as explained in section 2.1. We estimate the theoretical uncertainty using 7 point scale variation for both fixed-order NNLO results as well as MiNLO predictions. The scale variation in production and decay are always correlated (this includes the decay renormalisation scale, i.e. the scale at which we evaluate the $\overline{\mathrm{MS}}$ b-quark mass). We perform correlated variations in MCFM-8.0 and HZJ-MiNLO, that is, our final uncertainty is an envelop of 7 scale combinations, i.e. for a given (K_r, K_f) choice in HZJ-MiNLO we use the same choice in MCFM-8.0 and as usual we consider variations of the central scale by a factor two up and down, restricted to $1/2 \leq K_r/K_f < 2$. Note that when varying the renormalization scale in the MiNLO results we have also turned on the scale variation in the MiNLO Sudakov form factor. This scale variation effectively incorporates the uncertainty of the prediction related to the variation of the hard scale Q present in the Sudakov form factor in eq. (2.3). For more details see appendix B of ref. [26]. The $gg \to \mathrm{HZ}$ contribution is then added with the same (K_r, K_f) choice.

When interfacing our fixed-order predictions to a parton shower we use Pythia8 [49] with the Monash 2013 tune [50], as detailed more precisely in the next subsection. Unless stated otherwise, predictions are shown at parton level, with no multi-parton interactions. On top of the uncertainties discussed above, uncertainties connected to the merging and parton-shower matching could be probed by varying the choice of $h(p_t)$ in eq. (2.17), by using different parton showers or parton-shower tunes, by varying the radiation hardness for events with radiation far from singular limits, or by varying the splitting of the full real radiation into a singular and regular parts using the so-called hfact option. A complete assessment of these uncertainties is beyond the scope of this paper. However, comprehensive studies related to these uncertainties should be addressed in the future.

3.2 Interface to parton shower

In order to combine our results with a parton shower we follow an approach similar to the one first introduced for the NLO $t\bar{t}$ production treatment in [43], that allows for a generation of radiation also from resonances. In our simulation we set the flag allrad to 0, which means that the NLO POWHEG emission is generated at most from one singular region, associated either with the production stage or with the radiation from a resonance and we do not consider radiation from multiple regions. This is the standard POWHEG procedure to generate the hardest radiation. In this configuration POWHEG uses the usual highest bid mechanism to choose the origin of the emission. We remind the reader that by using the POWHEG-BOX-RES framework the phase space for emissions from resonances is treated appropriately, which means that the hard scale in the POWHEG-Sudakov is set by the allowed phase space for that emission.

For the parton shower we use Pythia8. A requirement for the matching to the parton shower to work properly is that the hardest radiation should be the one generated by POWHEG. This is usually achieved by setting a value of scalup in every event, which sets the starting scale for the parton shower. One subtlety is however that the definition of the hardness of the radiation from the decay in POWHEG and Pythia8 differ. As a consequence, after an event is showered, we recompute the hardness of the first emission generated by Pythia8 using the POWHEG formula and accept the showered event only if this hardness is lower than the scalup value of the given event. If this is not the case, we shower the event again until the new showered event meets the required condition. Details of the hardness definition used in POWHEG and Pythia8 are given in appendix A of ref. [43]. We have checked that our procedure to veto radiation gives results that are fully compatible with those obtained by the procedure encoded in the PowhegHooks-class provided by Pythia8 [49].

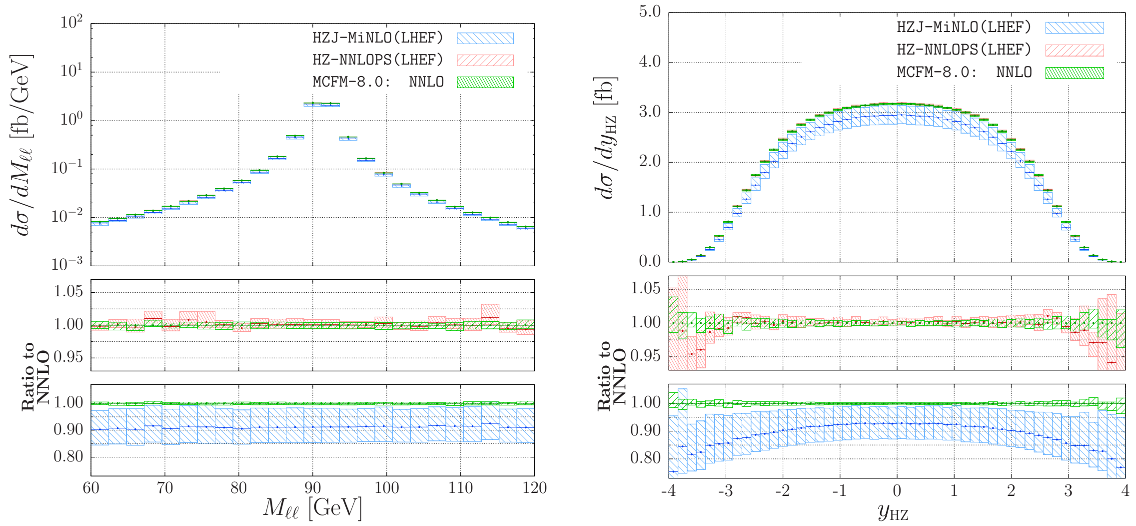

Figure 1. The differential distributions of the invariant mass of final-state leptons $M_{\ell\bar{\ell}}$ (left panel) and the distribution of the rapidity of the HZ system y_{HZ} (right panel). The one-loop squared terms from the $gg \to \mathrm{HZ}$ channel have not been included.

4 Validation

In the following section we present the validation of our results. We carefully compare distributions prepared from reweighted Les Houches events (`HZ-NNLOPS(LHEF)`) with the ones obtained using fixed-order NNLO code (`MCFM-8.0`). We remind the reader that, in the reweighting procedure, we don't take into account one-loop squared contributions arising from $gg \to \mathrm{HZ}$ channel, as specified and motivated in section 2.3 and 2.4 respectively. Therefore all the plots of this section do not contain the $gg \to \mathrm{HZ}$ channel, which instead will be included in section 5.

In the plots of this section, the blue, green and red markers represent results from `HZJ-MiNLO` Les Houches events, the fixed-order calculation obtained with `MCFM-8.0`, and the reweighted `HZ-NNLOPS(LHEF)` event sample, respectively. The uncertainty band represents the usual scale variation uncertainty, as described in detail in the previous section.

The first pair of plots that we want to present is the distribution of the invariant mass of final-state leptons $M_{\ell\bar{\ell}}$ and the distribution of the rapidity of the HZ system y_{HZ}, which are shown in the left and right panel of figure 1, respectively. We start by noting that the ratio of `MCFM-8.0` to `HZJ-MiNLO`, bottom panel of figure 1, is constant, which is along the lines of our assumption that the reweighting factor $\mathcal{W}(\Phi_{\ell\bar{\ell}b\bar{b}})$ should be constant along the $M_{\ell\bar{\ell}}$ direction. We do not repeat the thorough procedure of validation, which was included in our previous work [30]. The distribution of y_{HZ}, right panel of figure 1, is again properly reproduced by our calculation across the whole spectrum. We take note of the fact that the discrepancies at the edges of the distribution are in the regions of phase-space which are poorly populated. More precisely, having used distributions with varying bin-size for the reweighting, all events with $y_{\mathrm{HZ}} \lesssim -3$ (or $y_{\mathrm{HZ}} \gtrsim +3$) fall into the first (or the last) bin of the differential reweighting factor $\mathcal{W}(\Phi_{\ell\bar{\ell}b\bar{b}})$. The description of the forward rapidity region

JHEP11(2018)157

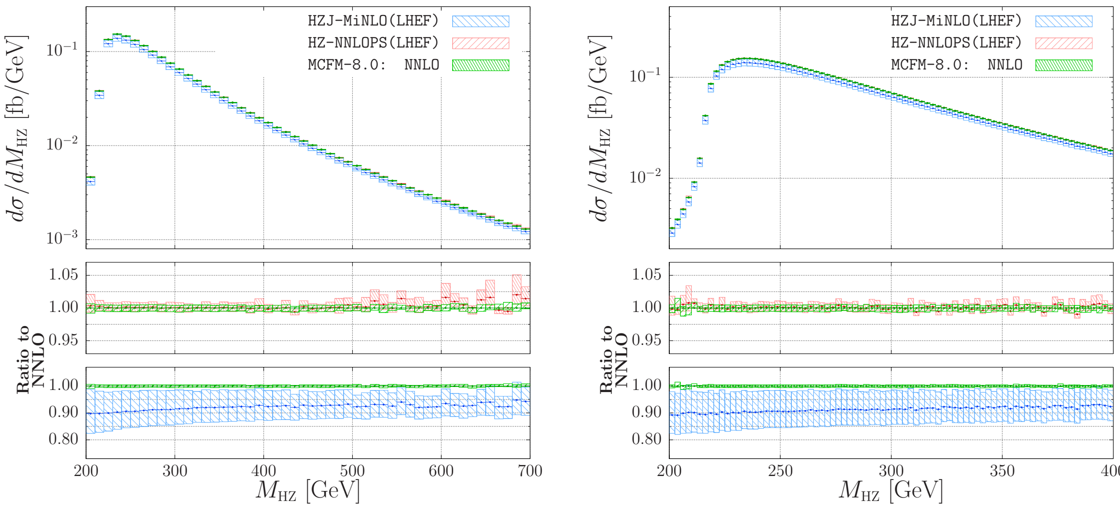

Figure 2. The differential distributions of the invariant mass of the HZ system $M_{\rm HZ}$ in two different mass regions. The one-loop squared terms from $gg \to$ HZ channel have not been included.

can be improved by increasing the statistics of the multi-differential distributions and by including more bins at large rapidity. In figure 2, we present the differential distribution of $M_{\rm HZ}$ in two different mass regions. For this distribution the difference between `HZJ-MiNLO` and the NNLO is small and flat over the whole range. After reweighting, we find perfect agreement between NNLO and `HZ-NNLOPS(LHEF)` results.

As the next step, we look closely at the differential distributions of the angular variables: cosα and Collins-Soper angles. The distribution of cosα is presented in figure 3. We recollect that this dependence was not just recorded as a histogram, but rather parametrised in terms of spectral modes, eq. (2.13). This has improved the stability of the distribution, and as a consequence of the reweighting factor, which is very useful when working with samples of limited statistics. In summary, we find that for all variables used for the reweighting, the NNLO and `HZ-NNLOPS(LHEF)` predictions agree within their statistical fluctuations. Further we check the quality of the reconstruction of the Collins-Soper angles. We present the relevant distributions in figure 4.

To complete the validation, we also need to examine Born-like observables that were not used in the reweighting procedure. As such, we chose to look at transverse momentum and rapidity of the Higgs boson (see figure 5). We again confirm that both the central values and scale variation bands are properly reconstructed within statistical fluctuations, which increase at high transverse momentum ($p_{t,\rm H} \gtrsim 400$ GeV) and large rapidity ($|y_{\rm H}| \gtrsim 3$). The agreement between NNLO and `HZ-NNLOPS(LHEF)` in these corners of phase space could be improved further by increasing the statistics of the reweighting factor and decreasing the bin-sizes in this region.

Finally we turn to the discussion of the distribution of the transverse momentum of HZ system, an observable which is singular at Born level but receives corrections due to QCD radiation at higher-orders in perturbation theory. We compare results obtained using two different reweighting prescriptions: the one described in section 2.3, presented in the

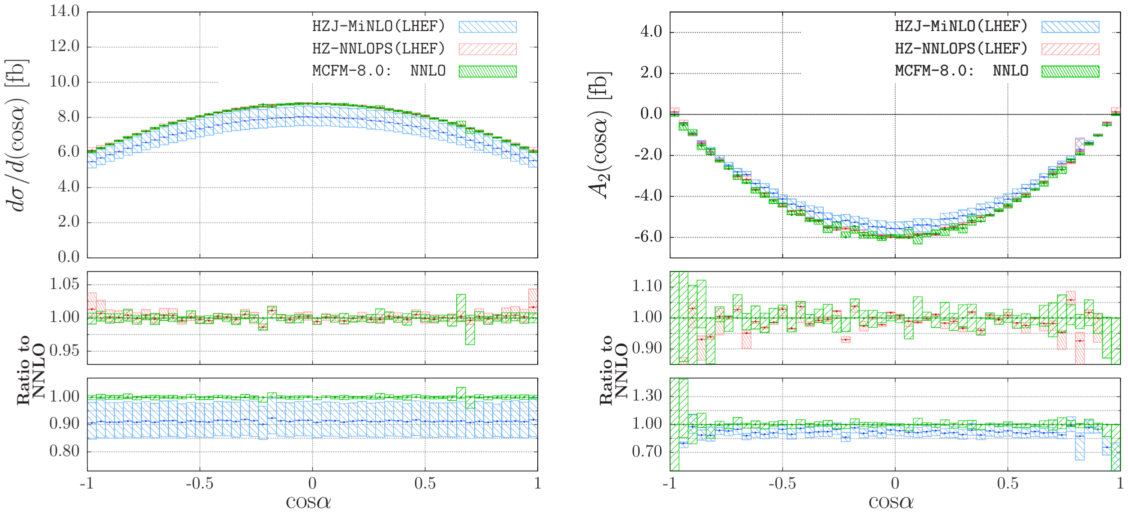

Figure 3. The differential distributions of the Z boson polar angle with respect to the beam axis, defined in eq. (2.9): differential cross section as a function of $\cos\alpha$ (left panel) and the dependence of coefficient $A_2(\cos\alpha)$, see eq. (2.11). The one-loop squared terms from the $gg\to$HZ channel have not been included.

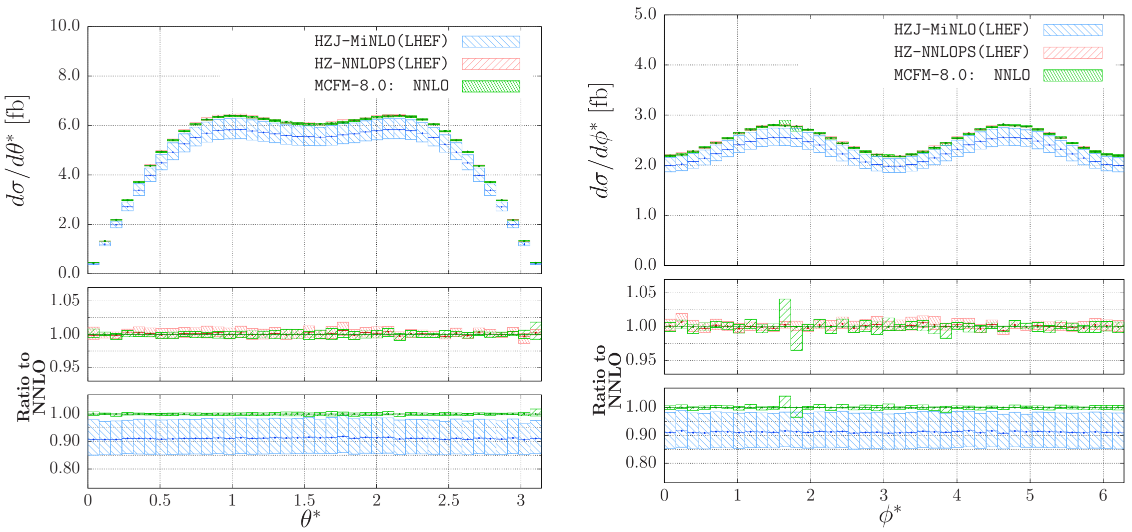

Figure 4. The differential distributions of Collins-Soper angles: θ^* (left) and ϕ^* (right). The one-loop squared terms from the $gg\to$HZ channel have not been included.

left plot of figure 6, and a setup where we set the function $h(p_t) \equiv 1$ in eqs. (2.15)–(2.17), shown in the right hand side of figure 6. As expected, we observe that the `HZJ-MiNLO` and `HZ-NNLOPS(LHEF)` predictions feature a Sudakov damping at low transverse momentum, while the NNLO prediction diverges in this region. Furthermore, we observe that for the $h(p_t) = 1$ case, the `HZ-NNLOPS(LHEF)` results are uniformly shifted with respect to the original event sample `HZJ-MiNLO`, as the reweighting factor $\mathcal{W}(\Phi_{\mathrm{H}\ell\bar{\ell}})$ does not take into account any QCD radiation. Instead, when the reweighting factor depends on the

JHEP11(2018)157

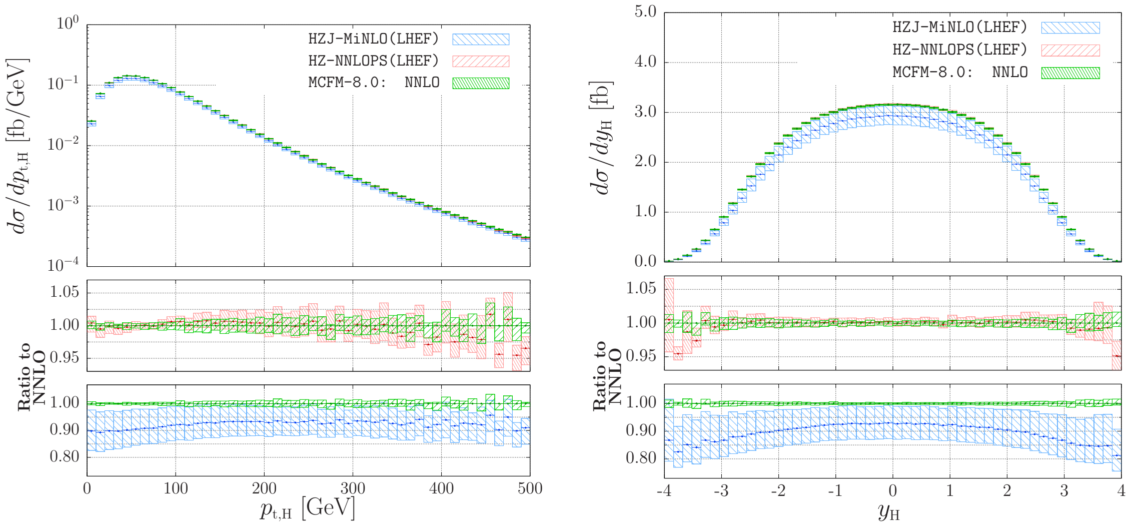

Figure 5. The differential distributions of the transverse momentum (left panel) and the rapidity (right panel) of the Higgs boson. The one-loop squared terms from the $gg \to \mathrm{HZ}$ channel have not been included.

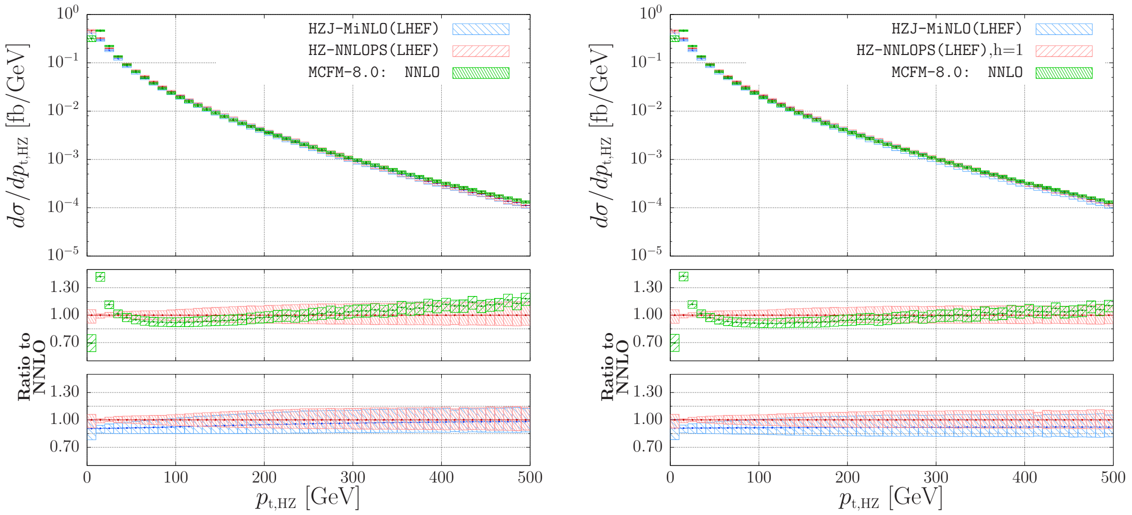

Figure 6. The differential distribution of the transverse momentum of the HZ system results when reweighting with damping factor $h(p_t)$ (left panel) or without (right panel). The one-loop squared terms from the $gg \to \mathrm{HZ}$ channel have not been included.

transverse momentum of the leading jet, `HZ-NNLOPS(LHEF)` approaches the `HZJ-MiNLO` curve at high-$p_{\mathrm{t,HZ}}$ values, as the effects of the reweighting are concentrated in the region of phase-space close to the Born kinematics, the natural habitat of $\mathcal{O}(\alpha_s^2)$ virtual corrections. In this case, the `HZ-NNLOPS(LHEF)` prediction at high transverse momentum agrees with the `HZJ-MiNLO` prediction, rather than with the pure NNLO result. We note that in this region, all predictions are only NLO accurate and that the former has a dynamical scale, dictated by the `MiNLO` prescription, while the NNLO uses a fixed renormalisation and factorisation

JHEP11(2018)157

Fiducial cross section	`HZJ-MiNLO`	`MCFM-8.0`	`HZ-NNLOPS(LHEF)`	`HZNNLOPS`
no $gg \to \mathrm{HZ}$	$6.59^{+7.2\%}_{-6.2\%}$ fb	$7.14^{+0.5\%}_{-0.9\%}$ fb	$7.14^{+0.3\%}_{-0.4\%}$ fb	$6.49^{+0.8\%}_{-0.6\%}$ fb
with $gg \to \mathrm{HZ}$	–	$7.92^{+2.0\%}_{-1.5\%}$ fb	$7.90^{+2.8\%}_{-2.0\%}$ fb	$7.16^{+3.1\%}_{-2.1\%}$ fb
no $gg \to \mathrm{HZ}$, high-$p_{t,Z}$	$1.13^{+5.9\%}_{-5.3\%}$ fb	$1.21^{+0.1\%}_{-0.2\%}$ fb	$1.21^{+0.2\%}_{-0.3\%}$ fb	$1.13^{+1.5\%}_{-1.2\%}$ fb
with $gg \to \mathrm{HZ}$, high-$p_{t,Z}$	–	$1.49^{+5.3\%}_{-4.1\%}$ fb	$1.48^{+5.3\%}_{-4.0\%}$ fb	$1.42^{+6.9\%}_{-5.1\%}$ fb

Table 1. Fiducial cross section of $pp \to \mathrm{HZ} \to \left(b\bar{b}\right)\left(e^+e^-\right)$ at 13 TeV with leptonic and b-jet cuts. The uncertainty band refers to the scale variation described in the text. Numerical errors for each prediction are beyond the quoted digits.

scale choice, $M_\mathrm{H} + M_\mathrm{Z}$. Comparing the middle panels of figure 6, it might seem that the choice of a uniform reweighting provides a better description of the hard part of $p_{t,\mathrm{HZ}}$ distribution, but the apparent agreement between `MCFM-8.0` and `HZ-NNLOPS(LHEF)` results around 400–500 GeV is accidental. In fact, at even higher transverse momenta the NNLO result is above our `HZ-NNLOPS(LHEF)` prediction. This behaviour is entirely due to the aforementioned difference in scale choice.

5 Phenomenological results

In this section we turn to the discussion of the phenomenological results obtained with our new code. We stress again that we consider the production of a Higgs boson in association with a Z boson and their subsequent decays $\mathrm{H} \to b\bar{b}$ and $\mathrm{Z} \to \ell^+\ell^-$, where in the following ℓ denotes a single leptonic species, e.g. e or μ. For the Higgs boson decay we include NLO QCD corrections.

We consider 13 TeV LHC collisions. We consider fiducial cuts inspired by the recent ATLAS analysis of ref. [3]. We require two charged leptons with $|y_\ell| < 2.5$ and $p_{t,\ell} > 7$ GeV, moreover the harder lepton should satisfy $p_{t,\ell} > 27$ GeV. We impose that the invariant mass of the leptons satisfies the condition 81 GeV $< M_{\ell\bar{\ell}} <$ 101 GeV. Additionally we require at least two b-jets with $|\eta_j| < 2.5$ and $p_{t,j} > 20$ GeV. Unless stated otherwise, jets are defined using the flavour-k_t algorithm [51] with $R = 0.4$. In the flavour-k_t algorithm we only consider b-quarks to be flavoured, and all other light quarks to be flavourless. Using b-tagging, such an algorithm can be implemented in experimental analyses. The fiducial cross sections in this phase-space volume at different levels of our simulations, are reported in table 1. We also present results with an additional cut on the Z boson transverse momentum, $p_{t,\mathrm{Z}} > 150$ GeV, which we refer to as high-$p_{t,\mathrm{Z}}$ region.

We first discuss the results without $gg \to \mathrm{HZ}$ contribution, over the full range of Z boson transverse momentum reported in the first line of the table 1. The `HZJ-MiNLO` cross section is about 8% smaller than the full NNLO calculation from `MCFM-8.0`. The difference is properly accounted for by reweighting the event sample and the cross section of `HZ-NNLOPS(LHEF)` and `MCFM-8.0` are equal to each other within the numerical accuracy (which is at the level of the last quoted digit). The scale uncertainty from the NLO result is reduced from about 7% to below 1% at the NNLO level. The inclusion of the $\mathcal{O}(\alpha_s^2)$ $gg \to \mathrm{HZ}$ channel, reported in the second line of the table, results in further increase of the total cross section by about 10%. In this case, the scale uncertainty is dominated by the new contribution, which is described only at leading order, and increases the scale uncertainty to the level of 2-3%. This larger scale uncertainty is somehow welcome, as a scale uncertainty below the percent level is unlikely to reflect the true perturbative uncertainty. This uncertainty will be reduced by an NLO treatment of the $gg \to \mathrm{HZ}$ contribution.[3]

We now discuss the impact of the parton shower on these cross sections. As is well known, in the presence of fiducial cuts that constrain the jet activity, as is in the case at hand, there can be a sizeable difference between a pure fixed-order computation and results after applying a parton shower. This is illustrated in the last two columns of the table. The parton shower allows for extra QCD radiation off coloured partons which can move the b-jets outside the fiducial phase-space volume, thereby reducing the recorded cross section. The impact of parton shower is similar in both instances, with and without the $gg \to \mathrm{HZ}$ contribution, and amounts to about 10% reduction of the cross section in the fiducial region, while the impact is milder, $5-7\%$, in the high-$p_{\mathrm{t,Z}}$ region.

If we now examine the results with an additional $p_{t,\mathrm{Z}}$ cut, reported in the last two lines of the table, we observe a reduction of the cross section by a factor of about 5 and in general behaviours similar to the ones described above. One point to note is that the impact of the $gg \to \mathrm{HZ}$ contribution is larger in this phase space region, which implies also larger scale uncertainties.

To further illustrate the effect of the $gg \to \mathrm{HZ}$ channel, we present in figure 7 the differential distributions of the invariant mass of the HZ system and transverse momentum of the b-jet pair system ($p_{\mathrm{t,b\bar{b}}}$) associated to the reconstruction of the Higgs boson momentum. To define the HZ-invariant mass we use the Monte Carlo truth, while $p_{\mathrm{t,b\bar{b}}}$ is obtained by clustering events with the flavour-k_t algorithm with $R = 0.4$ and by summing the transverse momenta of the two b-jets. If more than two b-flavoured jets are found, one selects the pair whose invariant mass is closest to the Higgs invariant mass.[4] We show results from the `HZNNLOPS` simulation before and after the inclusion of the $gg \to \mathrm{HZ}$ contribution (blue and red respectively) together with the fixed-order NNLO prediction including the $gg \to \mathrm{HZ}$ contribution (green). For the invariant mass distribution, the large impact of the $gg \to \mathrm{HZ}$ contribution above the top threshold is evident. Similarly, the transverse momentum distribution is mostly affected by the $gg \to \mathrm{HZ}$ contribution in the region between 150 and 200 GeV. In both cases the impact of $gg \to \mathrm{HZ}$ remains large up to high scales.

The invariant mass distribution (left panel of figure 7) features an almost uniform shift between the fixed-order predictions (green) and the ones including parton shower evolution (red). As discussed in the previous paragraph, parton shower leads to a decrease in the fiducial cross section mainly due to the b-jet cuts. However, the HZ invariant mass is not

[3]Note that the small difference in the $gg \to \mathrm{HZ}$ contribution in `MCFM-8.0` and `HZ-NNLOPS(LHEF)` is due to using `LHAPDF` or `POWHEG` routines to perform the running of the coupling from M_{Z} to the central scale choice $M_{\mathrm{H}} + M_{\mathrm{Z}}$.

[4]We do not distinguish between b and $\bar{b}$ jets.

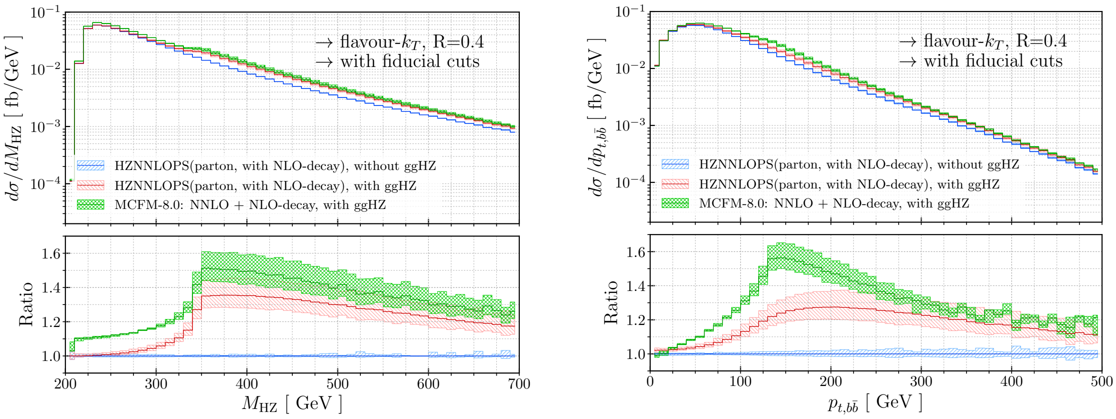

Figure 7. The differential distributions of the invariant mass of the HZ system (left panel) and the transverse momentum of the Higgs boson reconstructed from b-jets (right panel). The lower panel illustrate ratio of full results (NNLO as well as NNLOPS) to the NNLOPS results without $gg \to \mathrm{HZ}$ contribution.

strictly correlated with the Higgs kinematics (and hence with the b-jets from its decay). As a consequence, we observe a moderate and constant difference between `MCFM-8.0` and `HZNNLOPS`.

On the other hand, the effect of the parton shower on the transverse momentum of the reconstructed Higgs boson (right plot of figure 7) is quite different. In this case, one can see that the parton shower has a sizeable effect for $p_{t,b\bar{b}} \gtrsim 120\,\mathrm{GeV}$, and that it smears the distribution in a non-uniform way. At larger values of $p_{t,b\bar{b}} \gtrsim 300\,\mathrm{GeV}$, the effect of the partons shower becomes much more modest. A more detailed discussion is presented in appendix D.

As a next step, we want to study the quality of the Higgs boson reconstruction. In figure 8, we present a comparison of the transverse momentum distribution of the true Higgs boson, obtained using the momentum passed from the event generator before it splits to b-quarks and before any radiation off the b-quarks (labelled as `MC-truth`), and the $b\bar{b}$-jet system, reconstructed with a flavour-k_t algorithm as described above. We compare two sets of plots obtained with a jet radius of $R = 0.4$ (upper plots) or $R = 0.7$ (lower plots).[5] The plots show a comparison of the fixed-order results (green curve),[6] the `HZNNLOPS` after parton shower evolution (red) and the MC-truth prediction obtained with `HZNNLOPS` after parton shower (blue). The baseline in the ratio plot is taken to be the latter. In the left panels the $gg \to \mathrm{HZ}$ contribution is not included, whereas its effect is included in right panels.

We start by examining the results without $gg \to \mathrm{HZ}$ contribution (left hand panels). We note that both the fixed-order (green) and the `HZNNLOPS` after parton shower (red) differ from the `MC-truth` result (blue). At low transverse momenta, this difference becomes smaller when a larger jet-radius is considered (left bottom panel), which suggests that the dominant reason for the difference is out-of-jet radiation from the $b\bar{b}$-final state. At

[5] We note that the fiducial cuts are applied on jets of $R = 0.7$ in this case.
[6] Note that here only the b-quarks from the Higgs decay are considered flavoured.

JHEP11(2018)157

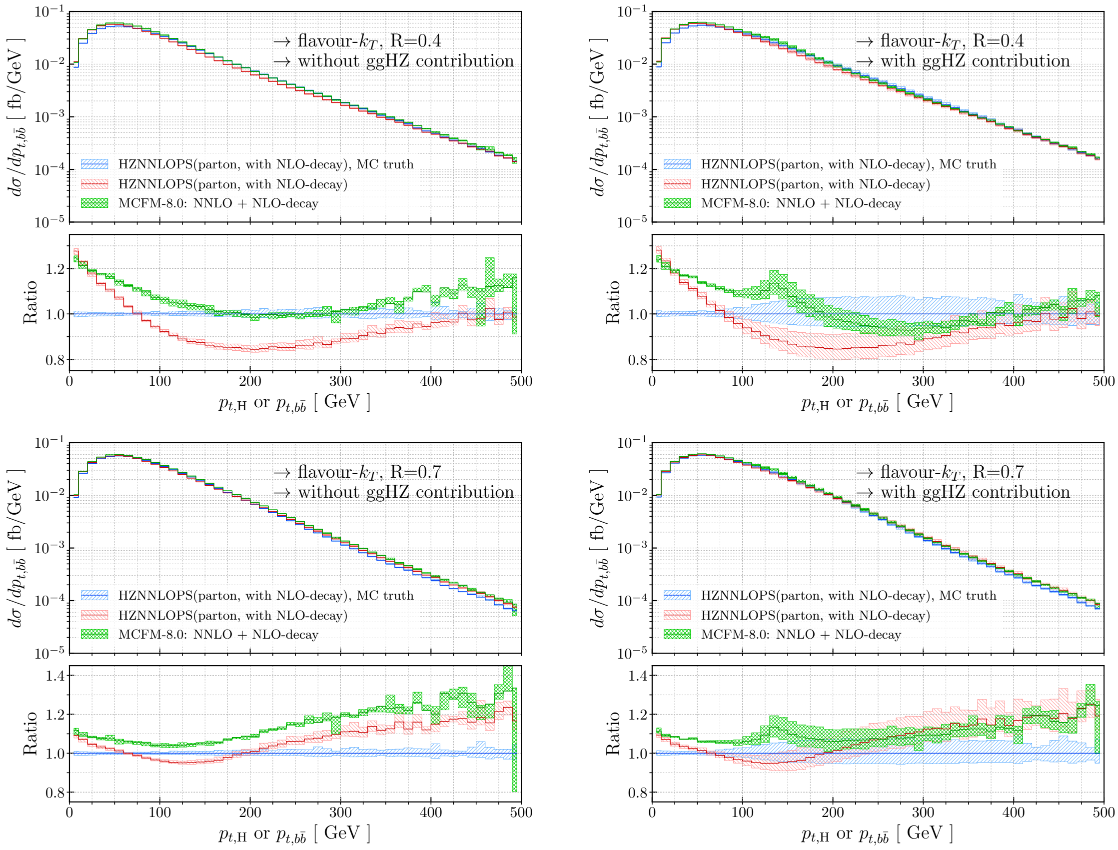

Figure 8. The differential distributions of the transverse momentum of the Higgs boson. `MC-truth` label refers to the actual Higgs boson momentum as passed from the event generator, other lines represent the reconstruction of the Higgs boson momentum using the two b-jets with invariant mass closest to M_{H}. The upper two plots show results for jets clustered with $R = 0.4$, the lower plots $R = 0.7$. Left plots do not include the $gg \to \mathrm{HZ}$ contribution, while the right plots do.

larger transverse momenta the difference with respect to the `MC-truth` is instead smaller at smaller jet-radius (top left panel), which points to the fact that in this region the difference is mainly due to radiation from the initial state. We also notice that in the intermediate transverse momentum region the fixed-order and `HZNNLOPS` show sizeable differences for $R = 0.4$, while these differences are more moderate when using $R = 0.7$. This can be easily understood from the fact that the observable with larger R is more inclusive and hence fixed-order and parton shower results are in better agreement.[7]

We now move to discuss the plots including the $gg \to \mathrm{HZ}$ effects. First, we note that the red and green bands in the top right panel if figure 8 are identical to the bands shown in the right panel of figure 7. As expected when the radius becomes bigger (bottom right panel) the fixed-order (green) and parton shower results (red) move closer to each other,

[7]When choosing instead a very large jet radius ($R > 1$) one would find again a larger difference between fixed-order and matched results. This is due to the fact that $R = 1$ treats initial and final state radiation democratically, while with a larger R one ends up clustering multiple initial-state radiation into jets.

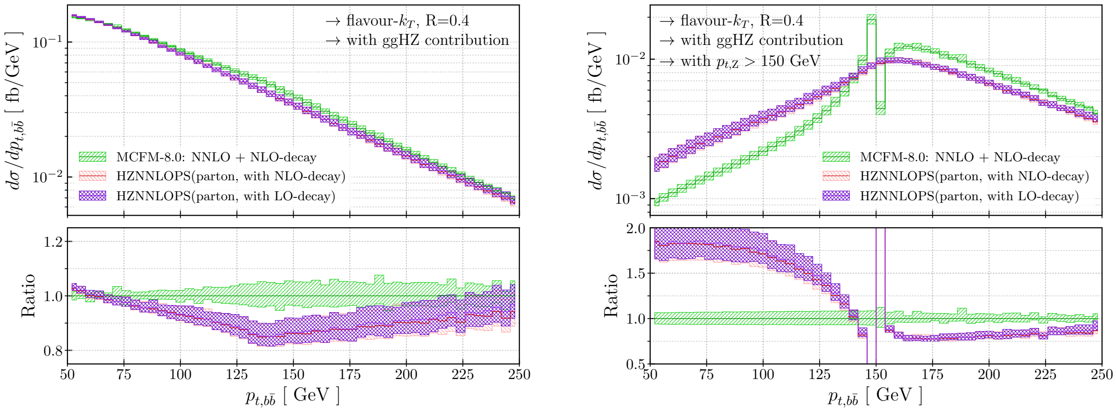

Figure 9. The differential distribution of the transverse momentum of the $b\bar{b}$-jet system without (left) and with (right) the cut $p_{\mathrm{t,Z}} > 150\,\mathrm{GeV}$. Results include the $gg \to \mathrm{HZ}$ contribution.

again because the observables become more inclusive. We also note that the uncertainty bands are now larger compared to the results without $gg \to \mathrm{HZ}$ contribution. This was already observed for the fiducial cross section and is due to the leading order description of the $gg \to \mathrm{HZ}$ contribution.

We now show the distribution of the transverse momentum of the $b\bar{b}$-jet system in the fiducial volume with and without the additional cut $p_{\mathrm{t,Z}} > 150\,\mathrm{GeV}$. The relevant plots are shown in figure 9. First of all we note that the difference between treating the $\mathrm{H} \to b\bar{b}$ decay at NLO with respect to LO is very small, which leads to the conclusion that a parton shower equipped with Matrix Element corrections to the $\mathrm{H} \to b\bar{b}$ branching provides a very good estimation of the higher-order corrections. We also notice a Sudakov shoulder in the fixed-order prediction in the right panel of figure 9 at $p_{\mathrm{t},b\bar{b}} = 150\,\mathrm{GeV}$. This feature has already been observed in figures (6) and (12) of ref. [9] and is due to the fact that the presence of the $p_{\mathrm{t,Z}} > 150\,\mathrm{GeV}$ cut makes the differential spectrum sensitive to soft gluon emission close to the cut. As expected, a parton shower captures parts of the resummation effects and therefore the shoulder is not present in the `NNLOPS` predictions.

One of the most important variables when reconstructing a resonance is the invariant mass of its decay products, therefore we will focus on it in the following, in the boosted high-$p_{\mathrm{t,Z}}$ region. At LO in the decay the $M_{b\bar{b}}$ distribution is an extremely narrow Breit-Wigner function, and receives sizeable corrections away from the peak only at higher-orders. We start by examining how well `Pythia8` can describe the decay of the Higgs boson by comparing two calculations that include LO or NLO decay in the matrix element. When the matrix element is computed at LO only, `Pythia8` includes the matrix element corrections and performs the shower using a hardness scale given in the Les Houches event file; the radiation from the decay of a heavy resonance is limited only by the phase space constraints of the particular emission. This comparison is shown in figure 10 without (left plot) and with $gg \to \mathrm{HZ}$ (right plot). We compare `HZNNLOPS` with LO treatment of the Higgs decay (purple), `HZNNLOPS` with NLO corrections to the $\mathrm{H} \to b\bar{b}$ decay (red) and `HZJ-MiNLO` predictions, with NLO decay (green).

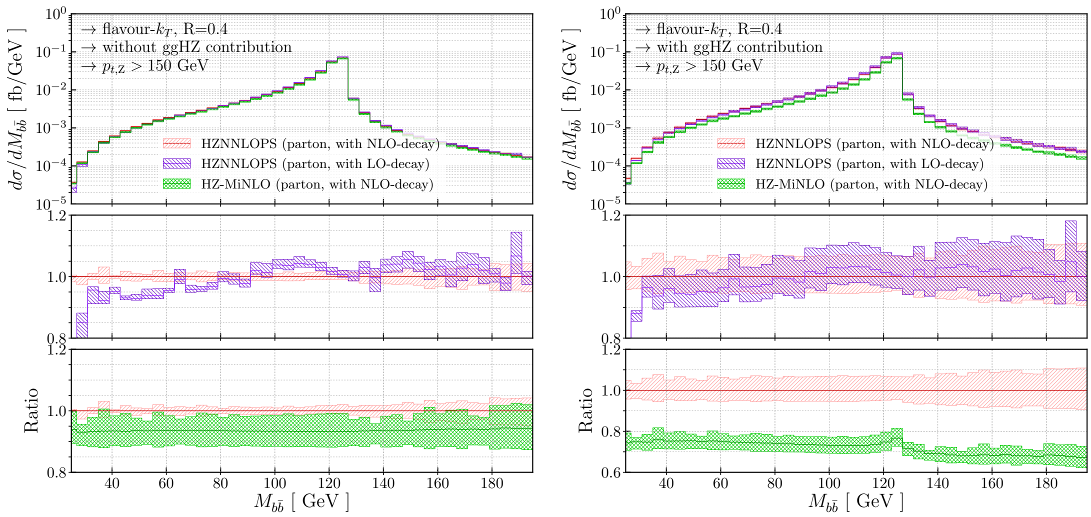

Figure 10. The differential distributions of the invariant mass of the $b\bar{b}$-system used for reconstruction of the Higgs boson. Comparison of HZNNLOPS results with LO and NLO decay matrix elements, excluding $gg \to \mathrm{HZ}$ channel (left panels) and with $gg \to \mathrm{HZ}$ (right panels).

We see that the two HZNNLOPS predictions are compatible with each other all the way down to relatively low $M_{b\bar{b}}$ masses. We note that the scale uncertainty is very small, of the order of 2-5%, when no $gg \to \mathrm{HZ}$ contribution is included. This uncertainty increases when $gg \to \mathrm{HZ}$ events are included, since these events, which sit at $M_{b\bar{b}} = M_{\mathrm{H}}$ before showering, carry a leading-order-like scale uncertainty that is spread to other bins by the parton shower. The small scale variation band is not indicative of the true uncertainty on this distribution and is related to the fact that HZJ-MiNLO results have been reweighted to NNLO results. In fact, the pure HZJ-MiNLO predictions, even without $gg \to \mathrm{HZ}$, have a larger uncertainty. We also note that this uncertainty is also somehow underestimated as the band does not cover the HZNNLOPS results. This is related to the well known fact that, in a plain POWHEG simulation, the scale is varied at the level of the $\bar{B}$ function, which is by definition inclusive over radiation, whereas the $M_{b\bar{b}}$ spectrum is sensitive to radiation.

In figure 11 we now compare fixed-order predictions (green) and our best prediction HZNNLOPS with NLO corrections to the $\mathrm{H} \to b\bar{b}$ decay (red). In the plots of figure 11 we show predictions obtained with b-jets clustered with $R = 0.4$ (top panels) and $R = 0.7$ (bottom panels). We point out that in order to populate the region to the left of the peak ($M_{b\bar{b}} < M_{\mathrm{H}}$) there must be a radiation off the b-quarks produced in the Higgs decay. On the contrary, the region on the right hand side of the peak ($M_{b\bar{b}} > M_{\mathrm{H}}$) is filled only when additional radiation, off the partons from the production stage, is clustered with the Higgs decay products.

In figure 11 we notice a sizeable enhancement in the $M_{b\bar{b}}$ distribution to the left of the Higgs peak. This enhancement was already observed in refs. [9, 21] and is even more dramatic in this case. If we compare our left plots to the figures (4) and (11) of ref. [9] we observe a larger K-factor. However there are a number of differences. First, the results of

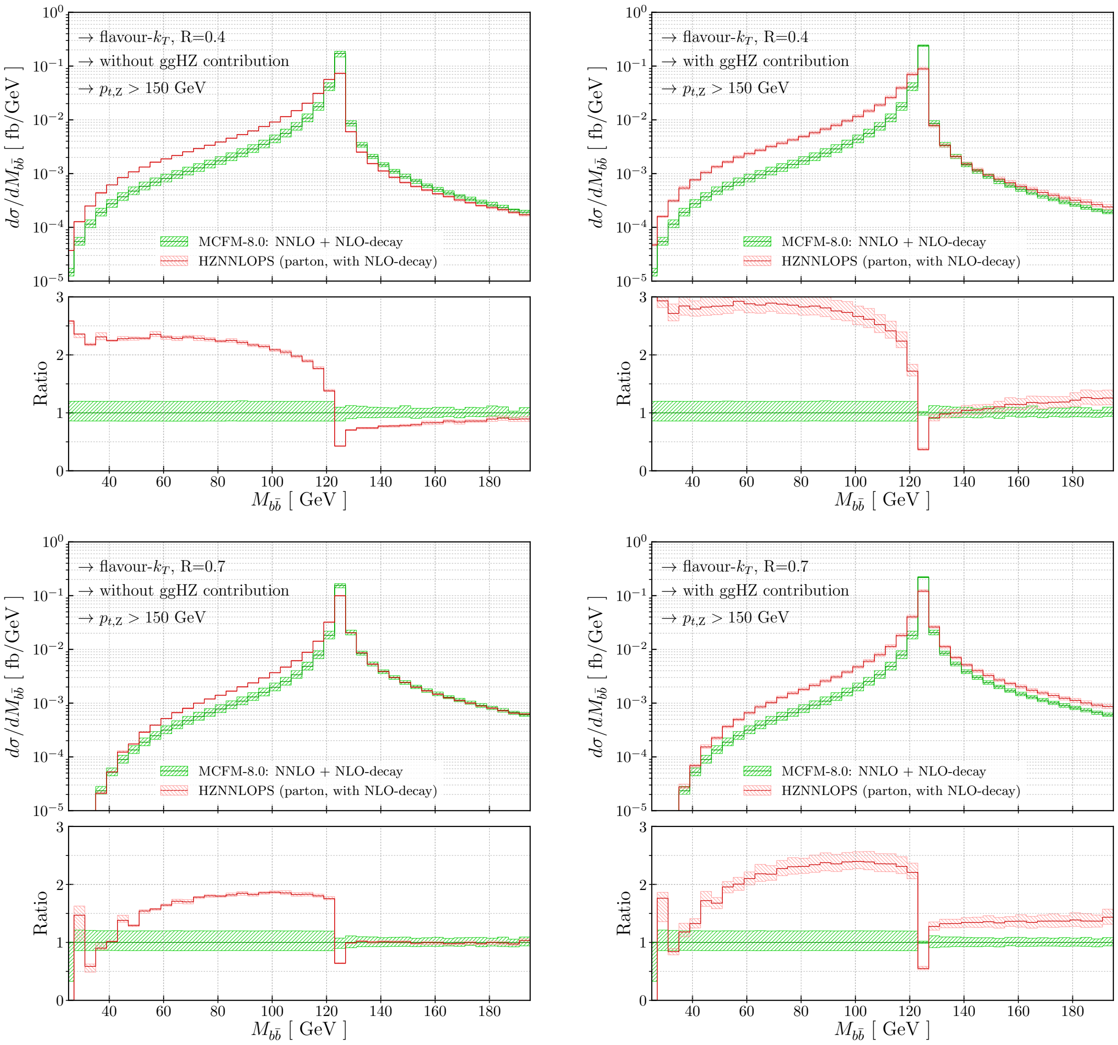

Figure 11. The differential distributions of the invariant mass of the $b\bar{b}$-system used for reconstruction of the Higgs boson. We present the results obtained with jet clustering with $R = 0.4$ (top) and $R = 0.7$ (bottom) excluding $gg \to$HZ channel (left panels) and with $gg \to$HZ (right panels).

ref. [9] are obtained with $R = 0.5$. Second, our `MCFM-8.0` predictions are obtained using massive b-quarks, while the NNLO-approx calculation shown in ref. [9] is obtained with massless b-quarks. Furthermore, the two computations use different fiducial cuts and in [9] the process HW^- is considered, rather than HZ. Last, our plots show `HZNNLOPS` results rather than `HZJ-MiNLO` ones, and from figure 10 this amounts to a further increase of the ratio by 10% (25%) without (with) $gg \to$HZ. Similar considerations apply when comparing to figure (2) of ref. [21].

By looking at the plots on the right of figure 11, one can observe an even more pronounced enhancement of the `HZNNLOPS` over the `MCFM-8.0` K-factor when the $gg \to$ HZ contribution is included. This is again due to the fact that the $gg \to$ HZ term in the fixed-order calculation is only in the $M_{b\bar{b}} = M_{\mathrm{H}}$ bin, while this contribution is spread to

JHEP11(2018)157

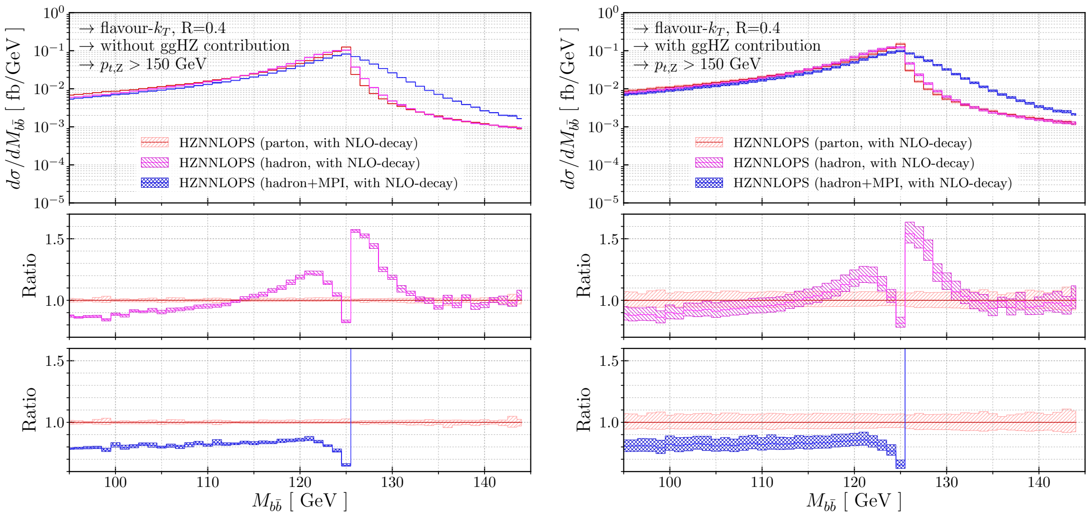

Figure 12. The differential distributions of the invariant mass of the $b\bar{b}$-system used for reconstruction of the Higgs boson. Comparison of `HZNNLOPS` results with NLO decay matrix elements at parton-, hadron-level and with multi-parton interactions (MPI), excluding $gg \to \mathrm{HZ}$ channel (left panels) and with $gg \to \mathrm{HZ}$ (right panels).

other bins by the parton shower. A second observation is that when a large jet radius is considered (bottom row), more radiation is clustered in the b-jets. As a consequence, the distribution vanishes faster away from M_{H}. This effect is stronger when a parton shower is included and causes the K-factor to be smaller to the left of the peak and to even become close to one at very low mass.

Finally, in figure 12 we present the $M_{b\bar{b}}$ distribution obtained with `HZNNLOPS` at various stages after the `Pythia8` parton showering, namely at parton-level and after hadronisation, with and without multi-parton interactions (MPI). We notice that hadronisation smears the distribution close to the peak. This is the reason for the dip at $M_{b\bar{b}} = M_{\mathrm{H}}$ in the first inset. Away from the peak $M_{b\bar{b}} = M_{\mathrm{H}}$, we observe that hadronisation effects become more important at low invariant masses, while, as expected, they become negligible at large $M_{b\bar{b}}$. Since colour-connections tend to reduce spatial distances between partons during hadronisation, more radiation is clustered within the b-jets. This is the reason why the small $M_{b\bar{b}}$ regions are underpopulated with respect to predictions at parton level. This effect is similar with or without MPI. On the contrary, we can see a substantial change when considering MPI in the region $M_{b\bar{b}} > M_{\mathrm{H}}$. Since MPI provide more radiation activity, many additional hadrons can be clustered within the b-jets, thereby increasing the invariant mass of the $b\bar{b}$-system and causing migration of events from the region $M_{b\bar{b}} \approx M_{\mathrm{H}}$ to larger invariant masses.

6 Conclusions

In this paper we have implemented a consistent matching of NNLO accurate predictions for HZ production to parton shower, including the subsequent decay of the Z boson into pair of leptons and the NLO decay of the Higgs boson into pair of b-quarks. The `HZNNLOPS` generator we obtained allows for a fully-exclusive simulation of the HZ production in a hadronic collision maintaining the advantages of the NNLO fixed-order calculation and supplying it with resummation effects as provided by the matching to a parton shower.

In order to obtain this accuracy, we have extended the existing `HZJ-MiNLO` implementation to include the NLO corrections to the $\mathrm{H} \to b\bar{b}$ decay. The NNLO+PS matching procedure requires a reweighting of the `HZJ-MiNLO` events that is fully-differential in the HZ Born kinematics. By using properties of the matrix elements at hand, we have parametrised the latter using variables that allow to express the differential cross section in terms of a finite set of functions, thereby simplifying considerably the multi-differential reweighting procedure. We have also included in the simulation the loop-induced $gg \to \mathrm{HZ}$ channel that enters at $\mathcal{O}(\alpha_s^2)$, as it constitutes a sizeable part of the total cross section, and can give rise to substantial distortions of kinematic distributions.

In section 5, we have considered a setup similar to the one used in searches for the Higgs decay into b-quarks. We find that scale uncertainties are substantially reduced when the NNLO corrections are included. Moreover we notice that the cross section in the fiducial region is reduced by about 5-10% during parton shower evolution as a consequence of requiring two b-jets satisfying the fiducial cuts. This correction brings the final result outside the NNLO uncertainty band. This highlights the limitation of using the scale uncertainty as an estimate of the true theoretical error associated to missing higher orders, in particular when more exclusive fiducial cuts are applied. An NNLO+PS simulation allows one to capture some of these higher order effects, albeit with limited logarithmic accuracy.

As already noted in the literature, we also find that the $gg \to \mathrm{HZ}$ channel has a significant impact, especially for the $M_{\mathrm{HZ}} > 2m_t$ part of the spectrum. Moreover its presence has a very strong impact on the size of the scale uncertainty band. Since this contribution only enters at $\mathcal{O}(\alpha_s^2)$ level, in order to reduce this uncertainty one needs to include higher-order corrections to the discussed channel, which are currently unknown.

We also notice differences between distributions of the transverse momentum of the Higgs boson, computed using Monte Carlo truth, and the transverse momentum of the $b\bar{b}$-system identified and used for the reconstruction of the Higgs boson momentum. We point out that, especially when a large jet-radius is used, the amount of radiation clustered into b-jets leads to a harder p_T-spectrum than the one of the true Higgs boson.

Despite the consistency of the procedure we used in our simulation, we have obtained a large K-factor in the $M_{b\bar{b}} < M_{\mathrm{H}}$ region of the distribution of the invariant mass of the $b\bar{b}$-system. We also point out that the scale uncertainty of the `NNLOPS` prediction in this part of the spectrum is underestimated, due to known properties of the algorithm used by `POWHEG` to generate real radiation. These two issues will certainly require further studies. Including NNLO corrections to the $\mathrm{H} \to b\bar{b}$ decay and matching them to parton showers would also be desirable, as well as trying to incorporate NLO electroweak effects as obtained in ref. [13], or studying improved methods to generate radiation off b-quarks [52]. We leave this to future work.

Acknowledgments

We would like to thank Gavin Salam for providing a private implementation of the flavour-k_t algorithm [51]. We also are grateful to Fabrizio Caola and Gionata Luisoni for providing some results of ref. [9] for cross-checks and to John Campbell, Giancarlo Ferrera, Keith Hamilton, and Paolo Nason for useful discussions. This work was supported in part by ERC Consolidator Grant HICCUP (No. 614577). The work of ER is supported by a Marie Skłodowska-Curie Individual Fellowship of the European Commission's Horizon 2020 Programme under contract number 659147 PrecisionTools4LHC. WA and WB thank CERN for their hospitality while part of this work was done.

A Treatment of the $\mathrm{H}\to b\bar{b}$ decay at NLO

The NLO corrections to the Higgs boson decay into two fermions $f\bar{f}$ have been known for a long time [14–18]. We have included them in the `HZJ-MiNLO` generator by extending the lists of the flavour structures considered by the process at hand to contain $b\bar{b}$ and $b\bar{b}g$ from the Higgs decay; creating the lists for the corresponding resonance structures; and by modifying the functions `setborn`, `setvirtual`, and `setreal` to supply amplitudes for the decay. The virtual corrections have been stripped of infra-red and ultra-violet singularities as described in section 2.4 of [53]. The relevant formulae read

$$\left|\mathcal{M}^{(0)}_{Hbb}(p_H)\right|^2 = 2\sqrt{2}N_c G_F\, p_H^2 \beta^2\, m_b^2(\mu_r)\,, \tag{A.1}$$

$$\begin{aligned}
2\Re\Big(\mathcal{M}^{(0)}_{Hbb}(p_H)^*\mathcal{M}^{(1)}_{Hbb}(p_H)\Big) = {}& \left|\mathcal{M}^{(0)}_{Hbb}(p_H)\right|^2 C_F\left(\frac{\alpha_s}{2\pi}\right)\\
&\times\Bigg\{ -2-4\log(2)+\frac{1+\beta^2}{\beta}\left(\frac{2\pi^2}{3}+2\,\mathrm{Li}_2(\xi)\right)\\
&+\frac{1+\beta^2}{2\beta}\log(\xi)\Big[\log(\xi)+4\log(\beta)\Big]\\
&+\frac{1-\beta^2}{\beta}\Big[-2\log(\xi)\Big]+2\Big[\log(1-\beta)+\log(1+\beta)\Big]\\
&-\left[\frac{1+\beta^2}{\beta}\log(\xi)+2\right]\log\left(\frac{\mu_r^2}{p_H^2}\right)+\left[-3\log\left(\frac{m_b^2}{\mu_r^2}\right)+4\right]\Bigg\}\,,
\end{aligned}\tag{A.2}$$

$$\begin{aligned}
\left|\mathcal{M}^{(0)}_{Hbbg}(p_H,q_1,q_2)\right|^2 = {}& \left|\mathcal{M}^{(0)}_{Hbb}(p_H)\right|^2 C_F\left(\frac{\alpha_s}{2\pi}\right)\cdot\frac{4\pi^2}{p_\mathrm{H}^2\beta^2}\Bigg[8+4\frac{q_1\cdot k}{q_2\cdot k}+4\frac{q_2\cdot k}{q_1\cdot k}\\
&+\beta^2\left(\frac{p_\mathrm{H}^2}{q_1\cdot k}\frac{p_\mathrm{H}^2}{q_2\cdot k}-\frac{1}{2}\left(\frac{p_\mathrm{H}^2}{q_1\cdot k}\right)^2-\frac{1}{2}\left(\frac{p_\mathrm{H}^2}{q_2\cdot k}\right)^2-4\frac{p_\mathrm{H}^2}{q_1\cdot k}-4\frac{p_\mathrm{H}^2}{q_2\cdot k}\right)\\
&+\beta^4\left(\frac{1}{2}\left(\frac{p_\mathrm{H}^2}{q_1\cdot k}\right)^2+\frac{1}{2}\left(\frac{p_\mathrm{H}^2}{q_2\cdot k}\right)^2+\frac{p_\mathrm{H}^2}{q_1\cdot k}\frac{p_\mathrm{H}^2}{q_2\cdot k}\right)\Bigg]\,,
\end{aligned}\tag{A.3}$$

where p_H is the momentum of Higgs boson, q_1 and q_2 are the momenta of the b and $\bar{b}$ quarks respectively, k is the momentum of the gluon in the real radiation matrix element,

$$x_b^2 = \frac{m_b^2}{p_H^2}, \quad \beta = \sqrt{1 - 4x_b^2}, \quad \text{and} \quad \xi = \frac{1-\beta}{1+\beta}. \tag{A.4}$$

With $m_b(\mu_r)$ we denote the b-quark mass in the $\overline{\text{MS}}$ scheme, evaluated at the decay renormalisation scale μ_r. For the case at hand, we pick the Higgs boson mass as the central value for μ_r and its variation is correlated with the production renormalisation scale variation, i.e. we use the same scaling factor for μ_r and μ_{R} (where the latter is the renormalisation scale used for the production matrix elements, as introduced in section 2.1). The last term in eq. (A.2) denotes a change from on-shell scheme to $\overline{\text{MS}}$ scheme, namely using eq. (63) of ref. [54] and retaining terms up to $\mathcal{O}(\alpha_s)$.

B Spectral decomposition of polar angle distributions

It is natural to use a spectral decomposition in terms of Fourier modes when dealing with an angular variable. The polar angle α that we use to parametrise the kinematics is defined on the interval $[0;\pi]$. The most generic parametrisation of the angular dependence can be written in terms of polynomials of $\cos\alpha$ and $\sin\alpha$ (note that quadratic and higher terms in $\sin\alpha$ can always be reduced to at most linear piece):

$$F(\alpha) = \sum_{a=0}^{\infty} \left(C_{1,a} (\cos\alpha)^a + C_{2,a} (\sin\alpha)(\cos\alpha)^a \right), \tag{B.1}$$

which equivalently reads

$$\begin{aligned} F(x) &= \sum_{a=0}^{\infty} \left(C_{1,a} x^a + C_{2,a} \left(\sqrt{1-x^2}\right) x^a \right) \\ &= \sum_{i=0}^{\infty} \bar{C}_i f_i(x) \end{aligned} \tag{B.2}$$

with

$$\begin{aligned} f_i(x) &= \left(\sqrt{1-x^2}\right)^{\text{mod(i,2)}} x^{\lfloor i/2 \rfloor}, \\ x &= \cos\alpha, \qquad x \in [-1;+1]. \end{aligned} \tag{B.3}$$

The above f_i functions are not orthonormal. Equipped with a scalar product between two functions

$$\langle F|G \rangle \equiv \int_{-1}^{+1} F(x)\, G(x)\, dx\,, \tag{B.4}$$

we can transform the basis of functions $\{f_i\}$ into an orthonormal set $\{g_j\}$ by means of a Gram-Schmidt recurrence relation

$$\begin{aligned} k = 0: &\quad \begin{cases} \tilde{g}_0 = & f_0, \\ g_0 = & \tilde{g}_0 / \langle \tilde{g}_0 | \tilde{g}_0 \rangle \end{cases} \\ k > 0: &\quad \begin{cases} \tilde{g}_k = & f_k - \sum_{j=0}^{k-1} \langle g_j | f_k \rangle \cdot g_j, \\ g_k = & \tilde{g}_k / \langle \tilde{g}_k | \tilde{g}_k \rangle \end{cases} \end{aligned} \tag{B.5}$$

JHEP11(2018)157

and express a generic function F in terms of the $\{g_j\}$ basis

$$F(x) = \sum_{j=0}^{N} c_j\, g_j(x)\,, \qquad \text{with} \qquad c_n = \langle g_n | F \rangle. \tag{B.6}$$

For the case at hand, due to the arguments given in appendix C, only terms up to $N = 10$ are needed.

C Hadronic tensor approach to matrix element

Hadronic collisions of protons are inherently linked with non-perturbative aspects of strong interactions through proton parton distribution functions (PDFs). Nevertheless we can use Lorentz symmetries and gauge invariance to predict the tensor structures that appear in matrix elements for associated Higgs production in pp collision. We distinguish two stages of the process: the production of the off-shell gauge boson in hadronic collision, that may be parametrised by the hadronic tensor, $H_{\mu\nu}$, and decay of the gauge boson into the Higgs boson and a pair of leptons, described by the decay tensor, $D_{\mu\nu}$. Since we are considering only QCD corrections and do not consider interference effects between production and decay products of the Higgs boson, the full squared matrix element can be written as

$$|\mathcal{M}(p_1, p_2, q, \ell_1, \ell_2)|^2 = \frac{H_{\mu\nu}(p_1, p_2, q) \cdot D^{\mu\nu}(q, \ell_1, \ell_2)}{\left(q^2 - M_Z^2\right)^2 + M_Z^2 \Gamma_Z^2}, \tag{C.1}$$

where p_1, p_2 are the momenta of the incoming protons, q is the momentum of the off-shell gauge boson before radiating off the Higgs boson, while ℓ_1 and ℓ_2 are the momenta of the two leptons that are produced. The momentum of the Higgs boson p_H may be obtained from conservation of momentum $p_H = q - \ell_1 - \ell_2$. We can parametrise the hadronic tensor as

$$H_{\sigma\sigma'} = (\varepsilon(q))^{\mu}_{\sigma}\; H_{\mu\nu}(p_1, p_2, q)\; (\varepsilon^*(q))^{\nu}_{\sigma'}\,, \tag{C.2}$$

where the ε-four-vectors denote polarisation tensors of the gauge boson in the amplitude and its conjugate part, corresponding to polarisations σ and σ' respectively. The most general covariant form for the hadronic tensor [55, 56] reads

$$\begin{aligned} H_{\mu\nu}(p_1, p_2, q) = {} & H_1 \left(g_{\mu\nu} - \frac{q_\mu q_\nu}{q^2} \right) + H_2\, \tilde{p}_{1\mu} \tilde{p}_{1\nu} + H_3\, \tilde{p}_{2\mu} \tilde{p}_{2\nu} \\ & + H_4 \big(\tilde{p}_{1\mu} \tilde{p}_{2\nu} + \tilde{p}_{2\mu} \tilde{p}_{1\nu} \big) + H_5 \big(\tilde{p}_{1\mu} \tilde{p}_{2\nu} - \tilde{p}_{2\mu} \tilde{p}_{1\nu} \big) \\ & + H_6 \epsilon(\mu\nu p_1 q) + H_7 \epsilon(\mu\nu p_2 q) \\ & + H_8 \big(\tilde{p}_{1\mu}\, \epsilon(\nu p_1 p_2 q) + \{\mu \leftrightarrow \nu\} \big) + H_9 \big(\tilde{p}_{2\mu}\, \epsilon(\nu p_1 p_2 q) + \{\mu \leftrightarrow \nu\} \big), \end{aligned} \tag{C.3}$$

where $\tilde{p}_{i\mu} = p_{i\mu} - (p_i q)/q^2 q_\mu$.

The decay tensor, $D_{\mu\nu}$, responsible for the part of the process that is represented inside a green circle in figure 13, can be parametrised as $D_{\sigma\sigma'} = (\varepsilon(q))_{\mu,\sigma}\; D^{\mu\nu}(q, \ell_1, \ell_2)\; (\varepsilon^*(q))_{\nu,\sigma'}$,

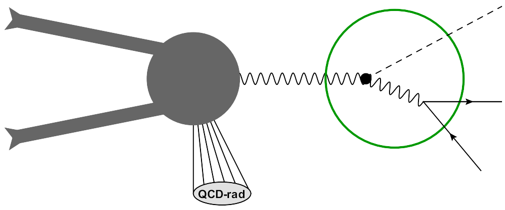

Figure 13. Amplitude for production of a weak gauge boson in proton-proton collision with subsequent branchings into Higgs boson and pair of leptons.

where $D^{\mu\nu}(q, \ell_1, \ell_2)$ has the structure (for simplicity we omit overall coupling constant factors)

$$D^{\mu\nu} = \frac{g^{\mu\alpha}\Big(-g_{\alpha\tilde{\alpha}} + \frac{k_\alpha k_{\tilde{\alpha}}}{M_Z^2}\Big) L^{\tilde{\alpha}\tilde{\beta}} \Big(-g_{\beta\tilde{\beta}} + \frac{k_\beta k_{\tilde{\beta}}}{M_Z^2}\Big) g^{\beta\nu}}{\left(k^2 - M_Z^2\right)^2 + M_Z^2\Gamma_Z^2}\,, \tag{C.4}$$

where $k = \ell_1 + \ell_2$ is the momentum of the gauge-boson after radiating off Higgs boson and

$$L^{\tilde{\alpha}\tilde{\beta}} = \mathrm{Tr}\left[\gamma^{\tilde{\alpha}}\left(V_\ell + A_\ell\gamma_5\right) \not{\ell}_1 \gamma^{\tilde{\beta}} \left(V_\ell + A_\ell\gamma_5\right) \not{\ell}_2\right], \tag{C.5}$$

where V_l and A_l are vector and axial components of the coupling of the vector boson to lepton. We can express the lepton momenta as $\ell_1 = \ell$ and $\ell_2 = k - \ell$. Plugging this into eq. (C.5) and then further into eq. (C.4), we find out that the momentum k of the Z boson after radiating off the Higgs boson appears in the final amplitude in eq. (C.1) with at most power 5. This argument is analogous to the one used in ref. [35] to obtain the general form of the angular dependence of Drell-Yan decays.

D Impact of the $gg \to$ HZ contributions

In this section we discuss the numerical impact of the loop-induced $gg \to$HZ contribution, that we include as explained in section 2.4. We will compare differential distributions obtained with the `HZNNLOPS` code and `MCFM-8.0`. The plots presented in this appendix show the result obtained at the level of Les Houches events before interfacing with parton shower. We will also comment on the differences with respect to the results after parton showering, shown in section 5.

The effect of the $gg \to$HZ contribution on the invariant mass of the HZ system is shown in figure 14, with the left and right panels showing the inclusive and fiducial distributions respectively. The distributions clearly show that, at LHEF level, the full `HZNNLOPS` result matches with `MCFM-8.0`, validating our procedure. One can also see that the $gg \to$ HZ contribution is significant when $M_{\rm HZ}$ is close to, or larger than, the $t\bar{t}$ threshold, and that the corrections remain large well above threshold. The application of fiducial cuts results in a further increase of the size of the corrections which is due to differences in acceptance rates for the two contributions (more than 60% $gg \to$HZ events pass the cuts compared to $\sim$ 45% `HZ-NNLOPS(LHEF)` events).

JHEP11(2018)157

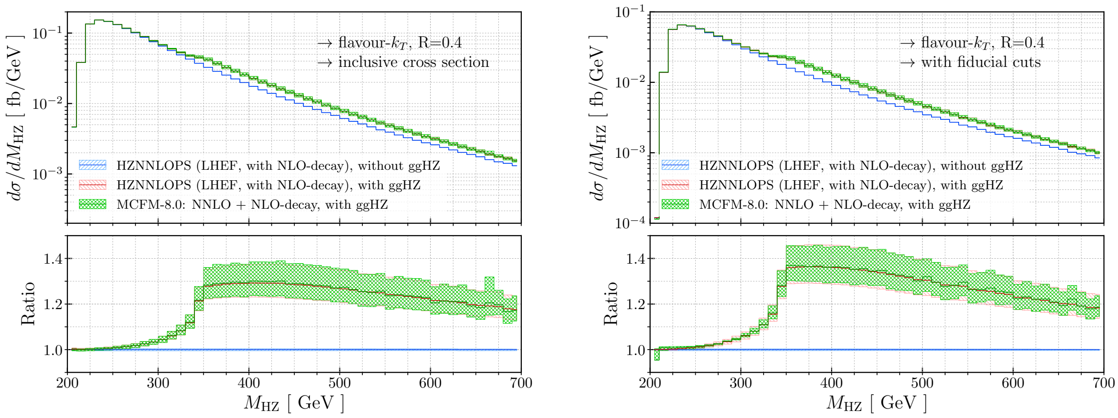

Figure 14. The differential distributions of the invariant mass of the HZ system at the LHEF level, without (left panel) and with fiducial cuts (right panel).

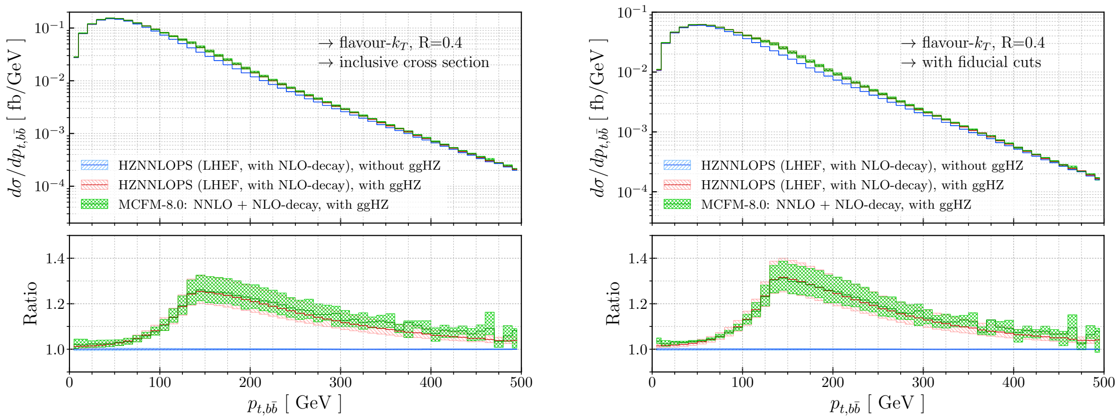

Figure 15. The differential distributions of the transverse momentum of the Higgs boson at the LHEF level, without (left panel) and with fiducial cuts (right panel).

Similar considerations apply to the distribution of transverse momentum of the Higgs boson reconstructed from two b-jets whose invariant mass is closest to the Higgs mass. These distributions are shown in figure 15. One noticeable difference is that the effect of the $gg \to$ HZ dies out faster at large transverse momentum.

JHEP11(2018)157

References

[1] ATLAS collaboration, *Observation of a new particle in the search for the Standard Model Higgs boson with the ATLAS detector at the LHC*, *Phys. Lett.* **B 716** (2012) 1 [arXiv:1207.7214] [INSPIRE].

[2] CMS collaboration, *Observation of a new boson at a mass of 125 GeV with the CMS experiment at the LHC*, *Phys. Lett.* **B 716** (2012) 30 [arXiv:1207.7235] [INSPIRE].

[3] ATLAS collaboration, *Evidence for the $H \to b\bar{b}$ decay with the ATLAS detector*, *JHEP* **12** (2017) 024 [arXiv:1708.03299] [INSPIRE].

[4] CMS collaboration, *Evidence for the Higgs boson decay to a bottom quark–antiquark pair*, *Phys. Lett.* **B 780** (2018) 501 [arXiv:1709.07497] [INSPIRE].

[5] G. Heinrich, *QCD calculations for the LHC: status and prospects*, in *5th Large Hadron Collider Physics Conference (LHCP 2017) Shanghai, China, May 15-20, 2017*, 2017, arXiv:1710.04998 [INSPIRE].

[6] O. Brein, A. Djouadi and R. Harlander, *NNLO QCD corrections to the Higgs-strahlung processes at hadron colliders*, *Phys. Lett.* **B 579** (2004) 149 [hep-ph/0307206] [INSPIRE].

[7] G. Ferrera, M. Grazzini and F. Tramontano, *Associated ZH production at hadron colliders: the fully differential NNLO QCD calculation*, *Phys. Lett.* **B 740** (2015) 51 [arXiv:1407.4747] [INSPIRE].

[8] J.M. Campbell, R.K. Ellis and C. Williams, *Associated production of a Higgs boson at NNLO*, *JHEP* **06** (2016) 179 [arXiv:1601.00658] [INSPIRE].

[9] F. Caola, G. Luisoni, K. Melnikov and R. Röntsch, *NNLO QCD corrections to associated WH production and $H \to b\bar{b}$ decay*, *Phys. Rev.* **D 97** (2018) 074022 [arXiv:1712.06954] [INSPIRE].

[10] M.L. Ciccolini, S. Dittmaier and M. Krämer, *Electroweak radiative corrections to associated WH and ZH production at hadron colliders*, *Phys. Rev.* **D 68** (2003) 073003 [hep-ph/0306234] [INSPIRE].

[11] A. Denner, S. Dittmaier, S. Kallweit and A. Muck, *Electroweak corrections to Higgs-strahlung off W/Z bosons at the Tevatron and the LHC with HAWK*, *JHEP* **03** (2012) 075 [arXiv:1112.5142] [INSPIRE].

[12] A. Denner, S. Dittmaier, S. Kallweit and A. Mück, *HAWK 2.0: A Monte Carlo program for Higgs production in vector-boson fusion and Higgs strahlung at hadron colliders*, *Comput. Phys. Commun.* **195** (2015) 161 [arXiv:1412.5390] [INSPIRE].

[13] F. Granata, J.M. Lindert, C. Oleari and S. Pozzorini, *NLO QCD+EW predictions for HV and HV +jet production including parton-shower effects*, *JHEP* **09** (2017) 012 [arXiv:1706.03522] [INSPIRE].

[14] E. Braaten and J.P. Leveille, *Higgs Boson Decay and the Running Mass*, *Phys. Rev.* **D 22** (1980) 715 [INSPIRE].

[15] M. Drees and K.-i. Hikasa, *note on qcd corrections to hadronic Higgs decay*, *Phys. Lett.* **B 240** (1990) 455 [*Erratum ibid.* **B 262** (1991) 497] [INSPIRE].

[16] N. Sakai, *Perturbative QCD Corrections to the Hadronic Decay Width of the Higgs Boson*, *Phys. Rev.* **D 22** (1980) 2220 [INSPIRE].

JHEP11(2018)157

[17] P. Janot, *First Order QED and QCD Radiative Corrections to Higgs Decay Into Massive Fermions*, Phys. Lett. **B 223** (1989) 110 [INSPIRE].

[18] A.L. Kataev and V.T. Kim, *The Effects of the massless $O(\alpha_S^2)$, $O(\alpha\alpha_s)$, $O(\alpha^2)$ QCD and QED corrections and of the massive contributions to* $\Gamma(H^0 \to b\bar{b}$, hep-ph/9304282 [INSPIRE].

[19] C. Anastasiou, F. Herzog and A. Lazopoulos, *The fully differential decay rate of a Higgs boson to bottom-quarks at NNLO in QCD*, JHEP **03** (2012) 035 [arXiv:1110.2368] [INSPIRE].

[20] V. Del Duca, C. Duhr, G. Somogyi, F. Tramontano and Z. Trócsányi, *Higgs boson decay into b-quarks at NNLO accuracy*, JHEP **04** (2015) 036 [arXiv:1501.07226] [INSPIRE].

[21] G. Ferrera, G. Somogyi and F. Tramontano, *Associated production of a Higgs boson decaying into bottom quarks at the LHC in full NNLO QCD*, Phys. Lett. **B 780** (2018) 346 [arXiv:1705.10304] [INSPIRE].

[22] S. Höche, Y. Li and S. Prestel, *Drell-Yan lepton pair production at NNLO QCD with parton showers*, Phys. Rev. **D 91** (2015) 074015 [arXiv:1405.3607] [INSPIRE].

[23] S. Höche, Y. Li and S. Prestel, *Higgs-boson production through gluon fusion at NNLO QCD with parton showers*, Phys. Rev. **D 90** (2014) 054011 [arXiv:1407.3773] [INSPIRE].

[24] S. Alioli, C.W. Bauer, C. Berggren, F.J. Tackmann, J.R. Walsh and S. Zuberi, *Matching Fully Differential NNLO Calculations and Parton Showers*, JHEP **06** (2014) 089 [arXiv:1311.0286] [INSPIRE].

[25] K. Hamilton, P. Nason and G. Zanderighi, *MINLO: Multi-Scale Improved NLO*, JHEP **10** (2012) 155 [arXiv:1206.3572] [INSPIRE].

[26] K. Hamilton, P. Nason, C. Oleari and G. Zanderighi, *Merging H/W/Z + 0 and 1 jet at NLO with no merging scale: a path to parton shower + NNLO matching*, JHEP **05** (2013) 082 [arXiv:1212.4504] [INSPIRE].

[27] K. Hamilton, P. Nason, E. Re and G. Zanderighi, *NNLOPS simulation of Higgs boson production*, JHEP **10** (2013) 222 [arXiv:1309.0017] [INSPIRE].

[28] K. Hamilton, P. Nason and G. Zanderighi, *Finite quark-mass effects in the NNLOPS POWHEG+MiNLO Higgs generator*, JHEP **05** (2015) 140 [arXiv:1501.04637] [INSPIRE].

[29] A. Karlberg, E. Re and G. Zanderighi, *NNLOPS accurate Drell-Yan production*, JHEP **09** (2014) 134 [arXiv:1407.2940] [INSPIRE].

[30] W. Astill, W. Bizon, E. Re and G. Zanderighi, *NNLOPS accurate associated HW production*, JHEP **06** (2016) 154 [arXiv:1603.01620] [INSPIRE].

[31] P. Richardson and D. Winn, *Investigation of Monte Carlo Uncertainties on Higgs Boson searches using Jet Substructure*, Eur. Phys. J. **C 72** (2012) 2178 [arXiv:1207.0380] [INSPIRE].

[32] G. Luisoni, P. Nason, C. Oleari and F. Tramontano, *$HW^{\pm}/HZ + 0$ and 1 jet at NLO with the POWHEG BOX interfaced to GoSam and their merging within MiNLO*, JHEP **10** (2013) 083 [arXiv:1306.2542] [INSPIRE].

[33] T. Ježo and P. Nason, *On the Treatment of Resonances in Next-to-Leading Order Calculations Matched to a Parton Shower*, JHEP **12** (2015) 065 [arXiv:1509.09071] [INSPIRE].

JHEP11(2018)157

[34] S. Frixione, P. Nason and C. Oleari, *Matching NLO QCD computations with Parton Shower simulations: the POWHEG method*, JHEP **11** (2007) 070 [arXiv:0709.2092] [INSPIRE].

[35] J.C. Collins and D.E. Soper, *Angular Distribution of Dileptons in High-Energy Hadron Collisions*, Phys. Rev. **D 16** (1977) 2219 [INSPIRE].

[36] B. Hespel, F. Maltoni and E. Vryonidou, *Higgs and Z boson associated production via gluon fusion in the SM and the 2HDM*, JHEP **06** (2015) 065 [arXiv:1503.01656] [INSPIRE].

[37] D. Goncalves, F. Krauss, S. Kuttimalai and P. Maierhöfer, *Higgs-Strahlung: Merging the NLO Drell-Yan and Loop-Induced 0+1 jet Multiplicities*, Phys. Rev. **D 92** (2015) 073006 [arXiv:1509.01597] [INSPIRE].

[38] L. Altenkamp, S. Dittmaier, R.V. Harlander, H. Rzehak and T.J.E. Zirke, *Gluon-induced Higgs-strahlung at next-to-leading order QCD*, JHEP **02** (2013) 078 [arXiv:1211.5015] [INSPIRE].

[39] R.V. Harlander, A. Kulesza, V. Theeuwes and T. Zirke, *Soft gluon resummation for gluon-induced Higgs Strahlung*, JHEP **11** (2014) 082 [arXiv:1410.0217] [INSPIRE].

[40] C. Englert, M. McCullough and M. Spannowsky, *Gluon-initiated associated production boosts Higgs physics*, Phys. Rev. **D 89** (2014) 013013 [arXiv:1310.4828] [INSPIRE].

[41] R.V. Harlander, S. Liebler and T. Zirke, *Higgs Strahlung at the Large Hadron Collider in the 2-Higgs-Doublet Model*, JHEP **02** (2014) 023 [arXiv:1307.8122] [INSPIRE].

[42] R.V. Harlander, J. Klappert, C. Pandini and A. Papaefstathiou, *Exploiting the WH/ZH symmetry in the search for New Physics*, Eur. Phys. J. **C 78** (2018) 760 [arXiv:1804.02299] [INSPIRE].

[43] J.M. Campbell, R.K. Ellis, P. Nason and E. Re, *Top-Pair Production and Decay at NLO Matched with Parton Showers*, JHEP **04** (2015) 114 [arXiv:1412.1828] [INSPIRE].

[44] NNPDF collaboration, R.D. Ball et al., *Parton distributions for the LHC Run II*, JHEP **04** (2015) 040 [arXiv:1410.8849] [INSPIRE].

[45] L.A. Harland-Lang, A.D. Martin, P. Motylinski and R.S. Thorne, *Parton distributions in the LHC era: MMHT 2014 PDFs*, Eur. Phys. J. **C 75** (2015) 204 [arXiv:1412.3989] [INSPIRE].

[46] S. Dulat et al., *New parton distribution functions from a global analysis of quantum chromodynamics*, Phys. Rev. **D 93** (2016) 033006 [arXiv:1506.07443] [INSPIRE].

[47] S. Carrazza, J.I. Latorre, J. Rojo and G. Watt, *A compression algorithm for the combination of PDF sets*, Eur. Phys. J. **C 75** (2015) 474 [arXiv:1504.06469] [INSPIRE].

[48] K.G. Chetyrkin, J.H. Kuhn and M. Steinhauser, *RunDec: A Mathematica package for running and decoupling of the strong coupling and quark masses*, Comput. Phys. Commun. **133** (2000) 43 [hep-ph/0004189] [INSPIRE].

[49] T. Sjöstrand et al., *An Introduction to PYTHIA 8.2*, Comput. Phys. Commun. **191** (2015) 159 [arXiv:1410.3012] [INSPIRE].

[50] P. Skands, S. Carrazza and J. Rojo, *Tuning PYTHIA 8.1: the Monash 2013 Tune*, Eur. Phys. J. **C 74** (2014) 3024 [arXiv:1404.5630] [INSPIRE].

[51] A. Banfi, G.P. Salam and G. Zanderighi, *Infrared safe definition of jet flavor*, Eur. Phys. J. **C 47** (2006) 113 [hep-ph/0601139] [INSPIRE].

[52] L. Buonocore, P. Nason and F. Tramontano, *Heavy quark radiation in NLO+PS POWHEG generators*, Eur. Phys. J. **C 78** (2018) 151 [arXiv:1711.06281] [INSPIRE].

[53] S. Alioli, P. Nason, C. Oleari and E. Re, *A general framework for implementing NLO calculations in shower Monte Carlo programs: the POWHEG BOX*, *JHEP* **06** (2010) 043 [arXiv:1002.2581] [INSPIRE].

[54] J.M. Campbell, R.K. Ellis, F. Maltoni and S. Willenbrock, *Higgs-Boson production in association with a single bottom quark*, *Phys. Rev.* **D 67** (2003) 095002 [hep-ph/0204093] [INSPIRE].

[55] J.G. Korner and E. Mirkes, *Polarization density matrix of high q(T) gauge bosons in high-energy proton-anti-proton collisions*, *Nucl. Phys. Proc. Suppl.* **23B** (1991) 9 [INSPIRE].

[56] C.S. Lam and W.-K. Tung, *A Systematic Approach to Inclusive Lepton Pair Production in Hadronic Collisions*, *Phys. Rev.* **D 18** (1978) 2447 [INSPIRE].

JHEP11(2018)157